

**Supporting Information (SI)**

**Enantioseparation by High-performance Liquid  
Chromatography on Proline-Derived Helical Polyacetylenes**

*Ge Shi<sup>a,#</sup>, Xiao Dai<sup>b,#</sup>, Qian Xu<sup>a</sup>, Jun Shen<sup>b,\*</sup>, Xinhua Wan<sup>a,\*</sup>*

<sup>a</sup>Beijing National Laboratory for Molecular Sciences, Key Laboratory of Polymer Chemistry and Physics of Ministry of Education, College of Chemistry and Molecular Engineering, Peking University, Beijing 100871, China.

<sup>b</sup>Polymer Materials Research Center, Key Laboratory of Superlight Materials and Surface Technology, Ministry of Education, College of Materials Science and Chemical Engineering, Harbin Engineering University, Harbin 150001, China

<sup>#</sup>These authors contribute equally to this work.

\* Corresponding authors.

*E-mail addresses:* xhwan@pku.edu.cn (X. H. Wan); shenjun@hrbeu.edu.cn (J. Shen)

**Table of Contents**

1. <b>Experimental section.</b> Materials, instrumentation and analysis, synthesis procedures.....	2
2. <b><sup>1</sup>H/<sup>13</sup>C NMR and FTMS spectra of important compounds and polymers.....</b>	7
3. <b>Raman spectra of polymers.....</b>	27
4. <b>DSC curves of polymers.....</b>	28
5. <b>UV-Vis absorption and CD spectra.....</b>	28
6. <b>HPLC results .....</b>	32
7. <b>Computational simulation.....</b>	40
8. <b>Reference.....</b>	45

## 1. Experimental Section

**Materials.** HPLC solvents (tetrahydrofuran, *N,N*-Dimethylformamide, n-hexane and isopropanol), anhydrous solvents (dichloromethane and methanol) and common organic solvents were purchased from Xilong Scientific, Concord Technology, 3A Chemicals and Tongguang Chem. *N*-(*tert*-butoxycarbonyl)-(*S*)-prolinal was purchased from OuheChem. Isocyanate reagents were purchased from Energy Chemical, HEOWNS, and Shanghai Dibai Biotech. Racemates were purchased from Energy Chemical, Bide Pharmatech Ltd., HEOWNS, Accela, Shanghai Dibai Biotech and Aladdin.  $[\text{Rh}(\text{nbd})\text{Cl}]_2$  was purchased from Alfa Aesar. 4M HCl-dioxane was purchased from Energy Chemical. Dimethyl (1-Diazo-2-oxopropyl) phosphonate was purchased from Accela.  $\text{K}_2\text{CO}_3$ , NaCl and  $\text{Na}_2\text{SO}_4$  were purchased from Tongguang Chem. Wide-pore silica gel (Daiso gelSP-1000) with a mean particle size of 7  $\mu\text{m}$  and a mean pore-diameter of 100 nm, which was kindly supplied by Daiso Chemical (Osaka, Japan), was silanized using (3-aminopropyl)triethoxysilane in toluene at 80 °C.

### Instrumentation and Analysis.

NMR spectra were recorded on a Bruker ARX 400 instrument at ambient temperature using either  $\text{CDCl}_3$  or  $d_8$ -THF as the solvent and tetramethylsilane as the internal standard (400 MHz for  $^1\text{H}$ , and 101 MHz for  $^{13}\text{C}$ ). High-resolution mass spectra were obtained on a Bruker BIFLEX III mass spectrometer. The number-averaged molecular weight ( $M_n$ ), weight-averaged molecular weight ( $M_w$ ), and polydispersity index ( $M_w/M_n$ ) of polymer were estimated on a gel permeation chromatography (GPC) apparatus equipped with a Waters 2410 refractive index detector and a Waters 515 pump. THF was employed as the eluent at a flow rate of 1.0 mL/min at 25 °C. All GPC curves were calibrated against a series of monodispersed polystyrene standards. Thermogravimetric analyses (TGA) were carried out on a TA Instrument Q600 analyzer at a heating rate of 20 °C/min under a  $\text{N}_2$  flow rate of 100 mL/min. Laser Raman spectra were measured on a Thermo Scientific Nicolet NXR FT-Raman Spectrometer. UV-Vis absorption measurements were conducted on a Varian Cary 1E UV-Vis spectrometer. Optical rotations were recorded on a JASCO Model P-1030 digital polarimeter. Circular dichroism (CD) spectra were performed on a JASCO J-810 spectrometer. The light path length of the quartz cell used was 10 mm. The samples were dissolved in THF and DMF at a concentration of around  $1.0 \times 10^{-4}$  mol/L.

Chromatographic experiments were performed using a JASCO PU-2089 chromatograph equipped with UV-Vis (JASCO UV-2070) and circular dichroism (JASCO CD-2095) detectors at room temperature. A solution of a racemate (3 mg/mL) was injected into the chromatographic system through an intelligent sampler (JASCO AS-2055).

The 3D skeleton of polymeric stationary phase was conducted in the Material Studio software (version 5.0; Accelrys Software Inc.). First, the structures of repeated units were optimized using the geometry optimization of the Forcite module. To build polymer conformation, the dihedral angles of C-C-C-C and C=C-C=C, hereafter named  $\theta$  and  $\phi$ , were varied systematically in steps of 10°. The atactic polymers with 50 repeating units were then built up using Polymer Builder in the Material Studio, in which the dihedral angles were constrained to specific degrees. The structures were subjected to energy minimization with Smart Minimizer of the Discover module at first. Atomistic MD simulations were conducted with the Dynamics of Discover module with a NVT ensemble at 298 K. The total simulation time is 5.0 ps, and time step is 1 fs. The lowest energy 50-mer was only remained the middle 10 repeating units for the docking study.<sup>2</sup>

The docking study was carried out with AutoDock 4.2. The polymeric 10-units were loaded Gasteiger charges and calculated the affinity maps on a 70 × 70 × 70 (0.375 Å spaced) rectangular box centered on the target structure. The molecular docking of enantiomers was subjected to a total of 50 Lamarckian Genetic Algorithm runs. Set the population size and the number of energy evaluations to 150 and 2.5 million, respectively. The value of the initial coordinate for the center of the ligand, ligand rigid-body orientation, and relative dihedral angles were randomized each run. All conformations were then clustered to RMSD of 2.0, and ranked according to the relative free energy of binding (FEB). The average energy of the best cluster with the lowest docking energy result was chosen as the model for mechanism studies.<sup>3</sup>

### **Synthesis procedures.**

2-(*S*)-Acetenyl-*N*-(*tert*-butoxycarbonyl)-pyrrolidine (**mBoc**). The detailed synthetic process could be obtained from our previous work.<sup>1</sup> Yield: 90%. <sup>1</sup>H NMR (400 MHz, CDCl<sub>3</sub>,  $\delta$ , ppm): 4.62 - 4.32 (d, 1H, NCH), 3.56 - 3.18 (d, 2H, NCH<sub>2</sub>), 2.29-2.17 (m, 1H, C≡CH), 2.17 - 1.96 (t, 3H, CH<sub>2</sub>CH<sub>2</sub>), 1.96 - 1.81 (m, H, CH<sub>2</sub>). <sup>13</sup>C NMR (101 MHz, *d*-CDCl<sub>3</sub>,  $\delta$ , ppm): 154.0, 84.3, 79.7,

69.5, 47.9, 45.9, 45.4, 33.6, 32.9, 28.4, 24.4, 23.5. HRMS (m/z): [M+H]<sup>+</sup> calcd for C<sub>11</sub>H<sub>17</sub>NO<sub>2</sub>, 196.1259; found, 196.1327.

2-(*S*)-Acetenyl-*N*-(3', 5'-di(trifluoromethyl)phenyl)carbamoyl-pyrrolidine (**m2CF<sub>3</sub>**). Under the N<sub>2</sub> atmosphere, 4.0 g 2-(*S*)-Acetenyl-*N*-(*tert*-butoxycarbonyl)-pyrrolidine was added 35 mL 4 M HCl-dioxane in 150 mL round-bottom flask. After stirring for 2 h, the solvent was removed under vacuum. The residue was mixed with 40 mL anhydrous dichloromethane and 7 mL triethylamine at 0 °C. 7 g 3,5-di(trifluoromethyl)phenyl isocyanate was soluble in 15 mL anhydrous dichloromethane and added to the solution dropwise. After stirring for 24 h, the solution was washed by water and NaCl aqueous solution. The organic solution was dried by Na<sub>2</sub>SO<sub>4</sub> and filtered to remove salt. The crude product was obtained by the removal of solvent under reduced pressure and purified by column chromatography with ethyl acetate-petroleum ether mixtures as the eluent to yield 4.7 g of faint yellow solid. Yield: 66%. <sup>1</sup>H NMR (400 MHz, CDCl<sub>3</sub>, δ, ppm): 7.96 - 7.86 (m, 2H, ArH), 7.53 - 7.44 (m, 1H, ArH), 7.07 - 6.94 (m, 1H, NH), 4.63 - 4.46 (d, 1H, NCH), 3.65 - 3.44 (dt, 2H, NCH<sub>2</sub>), 2.53 - 2.45 (m, 1H, C≡CH), 2.32 - 2.08 (ddt, 3H, CH<sub>2</sub>CH<sub>2</sub>), 2.06 - 1.93 (dt, 1H, CH<sub>2</sub>). <sup>13</sup>C NMR (101 MHz, *d*-CDCl<sub>3</sub>, δ, ppm): 153.0, 140.5, 131.9, 124.6, 119.1, 116.1, 82.6, 73.1, 47.8, 46.3, 33.8, 24.1. HRMS (m/z): [M+H]<sup>+</sup> calcd for C<sub>15</sub>H<sub>12</sub>F<sub>6</sub>N<sub>2</sub>O, 351.1323; found, 351.0930.

2-(*S*)-Acetenyl-*N*-(3', 5'-dichlorophenyl)carbamoyl-pyrrolidine (**m2Cl**). Yield: 76%. <sup>1</sup>H NMR (400 MHz, CDCl<sub>3</sub>, δ, ppm): 7.43 - 7.35 (m, 2H, ArH), 7.03 - 6.98 (m, 1H, ArH), 6.82 - 6.65 (m, 1H, NH), 4.61 - 4.46 (d, 1H, NCH), 3.66 - 3.46 (dt, 2H, NCH<sub>2</sub>), 2.53 - 2.47 (m, 1H, C≡CH), 2.32 - 2.08 (ddt, 3H, CH<sub>2</sub>CH<sub>2</sub>), 2.06 - 1.93 (dt, 1H, CH<sub>2</sub>). <sup>13</sup>C NMR (101 MHz, *d*-CDCl<sub>3</sub>, δ, ppm): 152.9, 140.9, 135.0, 122.8, 117.5, 82.7, 72.5, 47.7, 46.2, 33.7, 24.1. HRMS (m/z): [M]<sup>+</sup> calcd for C<sub>13</sub>H<sub>12</sub>Cl<sub>2</sub>N<sub>2</sub>O, 283.2220; found, 283.0399.

2-(*S*)-Acetenyl-*N*-(3', 5'-dimethylphenyl)carbamoyl-pyrrolidine (**m2Me**). Yield: 82%. <sup>1</sup>H NMR (400 MHz, CDCl<sub>3</sub>, δ, ppm): 7.09 - 7.03 (m, 2H, ArH), 6.70 - 6.64 (m, H, ArH), 6.60 - 6.48 (m, 1H, NH), 4.60 - 4.47 (d, 1H, NCH), 3.61 - 3.45 (dt, 2H, NCH<sub>2</sub>), 2.48 - 2.43 (m, 1H, C≡CH), 2.31 - 2.25 (m, 6H, CH<sub>3</sub>), 2.23 - 2.09 (ddt, 3H, CH<sub>2</sub>CH<sub>2</sub>), 2.03 - 1.93 (dt, 1H, CH<sub>2</sub>). <sup>13</sup>C NMR (101 MHz, *d*-CDCl<sub>3</sub>, δ, ppm): 153.8, 138.8, 138.5, 124.7, 117.3, 83.3, 72.3, 47.7, 46.1, 33.8, 24.2, 21.4. HRMS (m/z): [M+H]<sup>+</sup> calcd for C<sub>15</sub>H<sub>18</sub>N<sub>2</sub>O, 243.1889; found, 243.1492.

2-(*S*)-Acetenyl-*N*-(4'-chlorophenyl)carbamoyl-pyrrolidine (**m<sup>4</sup>Cl**). Yield: 82%. <sup>1</sup>H NMR (400 MHz, CDCl<sub>3</sub>, δ, ppm): 7.42 - 7.33 (dt, 2H, ArH), 7.28 - 7.19 (dt, 2H, ArH), 6.75 - 6.61 (m, 1H, NH), 4.60 - 4.49 (d, 1H, NCH), 3.64 - 3.44 (dt, 2H, NCH<sub>2</sub>), 2.51 - 2.44 (m, 1H, C≡CH), 2.29 - 2.08 (ddt, 3H, CH<sub>2</sub>CH<sub>2</sub>), 2.06 - 1.93 (dt, 1H, CH<sub>2</sub>). <sup>13</sup>C NMR (101 MHz, *d*-CDCl<sub>3</sub>, δ, ppm): 153.5, 137.7, 128.8, 127.8, 120.8, 83.0, 72.6, 47.7, 46.1, 33.8, 24.1. HRMS (m/z): [M+H]<sup>+</sup> calcd for C<sub>13</sub>H<sub>13</sub>ClN<sub>2</sub>O, 249.1186; found, 249.0789.

2-(*S*)-Acetenyl-*N*-phenylcarbamoyl-pyrrolidine (**mPh**). Yield: 71%. <sup>1</sup>H NMR (400 MHz, CDCl<sub>3</sub>, δ, ppm): 7.46 - 7.36 (m, 2H, ArH), 7.33 - 7.23 (dd, 2H, ArH), 7.06 - 6.99 (t, 1H, ArH), 6.74 - 6.61 (m, 1H, NH), 4.61 - 4.49 (d, 1H, NCH), 3.63 - 3.44 (dt, 2H, NCH<sub>2</sub>), 2.49 - 2.42 (m, 1H, C≡CH), 2.28 - 2.07 (ddt, 3H, CH<sub>2</sub>CH<sub>2</sub>), 2.03 - 1.93 (dt, 1H, CH<sub>2</sub>). <sup>13</sup>C NMR (101 MHz, *d*-CDCl<sub>3</sub>, δ, ppm): 153.8, 139.0, 128.9, 123.0, 119.7, 83.2, 72.4, 47.7, 46.1, 33.8, 24.1. HRMS (m/z): [M+H]<sup>+</sup> calcd for C<sub>13</sub>H<sub>14</sub>N<sub>2</sub>O, 215.1576; found, 215.1176.

2-(*S*)-Acetenyl-*N*-(4'-methylphenyl)carbamoyl-pyrrolidine (**m<sup>4</sup>Me**). Yield: 73%. <sup>1</sup>H NMR (400 MHz, CDCl<sub>3</sub>, δ, ppm): 7.28 - 7.18 (d, 2H, ArH), 7.05 - 6.97 (d, 2H, ArH), 6.54 - 6.41 (m, 1H, NH), 4.53 - 4.41 (d, 1H, NCH), 3.56 - 3.38 (dt, 2H, NCH<sub>2</sub>), 2.40 - 2.35 (m, 1H, C≡CH), 2.26 - 2.19 (m, 3H, CH<sub>3</sub>), 2.18 - 2.00 (ddt, 3H, CH<sub>2</sub>CH<sub>2</sub>), 1.96 - 1.85 (dt, 1H, CH<sub>2</sub>). <sup>13</sup>C NMR (101 MHz, *d*-CDCl<sub>3</sub>, δ, ppm): 153.9, 136.4, 132.5, 129.4, 119.8, 83.3, 72.3, 47.7, 46.1, 33.8, 24.2, 20.8. HRMS (m/z): [M+H]<sup>+</sup> calcd for C<sub>14</sub>H<sub>16</sub>N<sub>2</sub>O, 229.17326; found, 229.1336.

2-(*S*)-Acetenyl-*N*-(4'-*tert*-butylphenyl)carbamoyl-pyrrolidine (**m<sup>t</sup>Bu**). Yield: 80%. <sup>1</sup>H NMR (400 MHz, CDCl<sub>3</sub>, δ, ppm): 7.36 - 7.27 (dd, 4H, ArH), 6.48 - 6.38 (m, 1H, NH), 4.59 - 4.48 (d, 1H, NCH), 3.62 - 3.46 (dt, 2H, NCH<sub>2</sub>), 2.46 - 2.42 (m, 1H, C≡CH), 2.28 - 2.07 (ddt, 3H, CH<sub>2</sub>CH<sub>2</sub>), 2.03 - 1.92 (dt, 1H, CH<sub>2</sub>), 1.33 - 1.24 (m, 9H, CCH<sub>3</sub>). <sup>13</sup>C NMR (101 MHz, *d*-CDCl<sub>3</sub>, δ, ppm): 153.9, 145.9, 136.3, 125.7, 119.5, 83.3, 72.4, 47.7, 46.1, 33.9, 31.4, 24.1. HRMS (m/z): [M+H]<sup>+</sup> calcd for C<sub>17</sub>H<sub>22</sub>N<sub>2</sub>O, 271.2202; found, 271.1809.

2-(*S*)-Acetenyl-*N*-(3'-chloro-4'-methylphenyl)carbamoyl-pyrrolidine (**m<sup>3</sup>Cl<sup>t</sup>Me**). Yield: 94%. <sup>1</sup>H NMR (400 MHz, CDCl<sub>3</sub>, δ, ppm): 7.55 - 7.46 (m, 1H, ArH), 7.23 - 7.16 (d, 1H, ArH), 7.14 - 7.06 (d, 1H, ArH), 6.71 - 6.56 (m, 1H, NH), 4.62 - 4.45 (d, 1H, NCH), 3.64 - 3.43 (dt, 2H, NCH<sub>2</sub>), 2.49 - 2.42 (m, 1H, C≡CH), 2.36 - 2.26 (m, 1H, CH<sub>3</sub>), 2.26 - 2.07 (ddt, 3H, CH<sub>2</sub>CH<sub>2</sub>), 2.03 - 1.92

(dt, 1H, CH<sub>2</sub>). <sup>13</sup>C NMR (101 MHz, *d*-CDCl<sub>3</sub>,  $\delta$ , ppm): 153.5, 137.9, 134.2, 130.8, 120.1, 117.9, 83.1, 72.5, 47.7, 46.1, 33.8, 24.2, 19.3. HRMS (*m/z*): [M+H]<sup>+</sup> calcd for C<sub>14</sub>H<sub>15</sub>ClN<sub>2</sub>O, 263.1342; found, 263.0949.

2-(*S*)-Acetenyl-*N*-(3'-chloro-5'-methylphenyl)carbamoyl-pyrrolidine (**m<sup>3</sup>Cl<sup>5</sup>Me**). Yield: 83%. <sup>1</sup>H NMR (400 MHz, CDCl<sub>3</sub>,  $\delta$ , ppm): 7.32 - 7.22 (m, 1H, ArH), 7.18 - 7.08 (m, 1H, ArH), 6.87 - 6.77 (m, 1H, ArH), 6.70 - 6.53 (m, 1H, NH), 4.58 - 4.46 (d, 1H, NCH), 3.62 - 3.46 (dt, 2H, NCH<sub>2</sub>), 2.51 - 2.45 (m, 1H, C $\equiv$ CH), , 2.31 - 2.26 (m, 1H, CH<sub>3</sub>), 2.26 - 2.08 (ddt, 3H, CH<sub>2</sub>CH<sub>2</sub>), 2.04 - 1.94 (dt, 1H, CH<sub>2</sub>). <sup>13</sup>C NMR (101 MHz, *d*-CDCl<sub>3</sub>,  $\delta$ , ppm): 153.4, 140.2, 139.9, 134.1, 123.7, 118.2, 116.6, 83.0, 72.7, 47.7, 46.2, 33.8, 24.1, 21.3. HRMS (*m/z*): [M+H]<sup>+</sup> calcd for C<sub>14</sub>H<sub>15</sub>ClN<sub>2</sub>O, 263.1342; found, 263.0944.

### **Polymerization.**

Monomer m2CF<sub>3</sub> (7.2 mmol, 2.5 g) and THF (16.5 mL) were added to a dry ampule. After three freeze-pump-thaw cycles, to the ampule was added a solution of [Rh(nbd)Cl]<sub>2</sub> (66 mg, 0.143 mmol) and TEA (1.5 mL) in THF (2.0 mL). The concentrations of monomer and the rhodium catalyst were 0.36 and 0.0072 M, respectively. The color of the reaction mixture turned dark red within 1 h. After stirring for 24 h at 30°C, the resulting polymer was precipitated into a large amount of methanol and collected by filtration and washed by methanol. After drying under vacuum at room temperature for 24 h, 1.8 g of paint yellow solids p2CF<sub>3</sub> were obtained. Yield: 74%. The other polymers were with the same synthetic procedure as p2CF<sub>3</sub>. All the polymers showed good solubility in THF and slight solubility in DMF. p<sup>3</sup>Cl<sup>5</sup>Me and p<sup>t</sup>Bu were slightly soluble in isopropanol so the HPLC eluent solvent for these two was pure *n*-hexane.

### **Preparation of chiral stationary phase.**

Taking p2CF<sub>3</sub> for example, 0.2 g p2CF<sub>3</sub> was dissolved in THF, then coated on 0.8 g aminopropyl silanized silica gel according to previous method.<sup>4</sup> The fed ratio between p2CF<sub>3</sub> to silica gel was 1:4 for p2CF<sub>3</sub>-based CSPs. The silica gels coated with polymers were packed in a stainless-steel tube (25 × 0.20 cm i.d.) by a slurry technique. The plate numbers of the packed columns were 1300–2500 for benzene using a hexane/2-propanol (90/10, v/v) mixture as the eluent at a flow rate

of 0.1 mL/min. 1,3,5-Tri-*t*-butylbenzene was used as a non-retained compound to estimate the dead time ( $t_0$ ). The retention time of enantiomers is  $t_1$  and  $t_2$ . The retention factor  $k_1 = (t_1 - t_0) / t_0$ , the separation factor  $\alpha = (t_2 - t_0) / (t_1 - t_0)$ .

## 2. $^1\text{H}/^{13}\text{C}$ NMR and FTMS Spectra of Important Compounds and Polymers

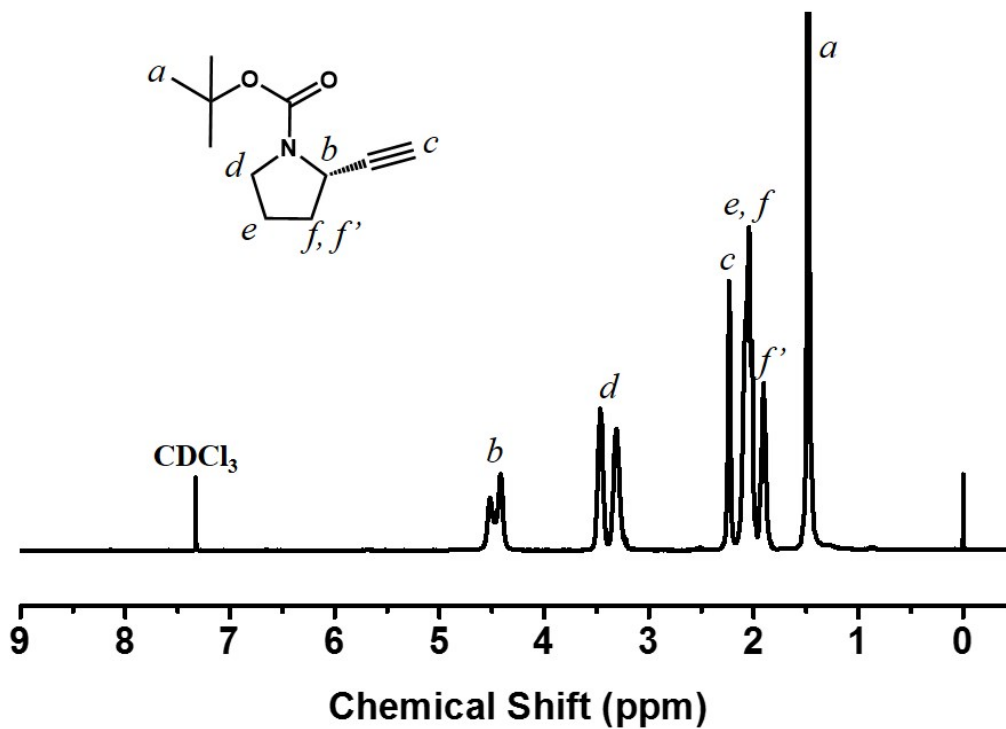


**Figure S1.**  $^1\text{H}$  NMR spectrum of mBoc measured in  $\text{CDCl}_3$  at room temperature.

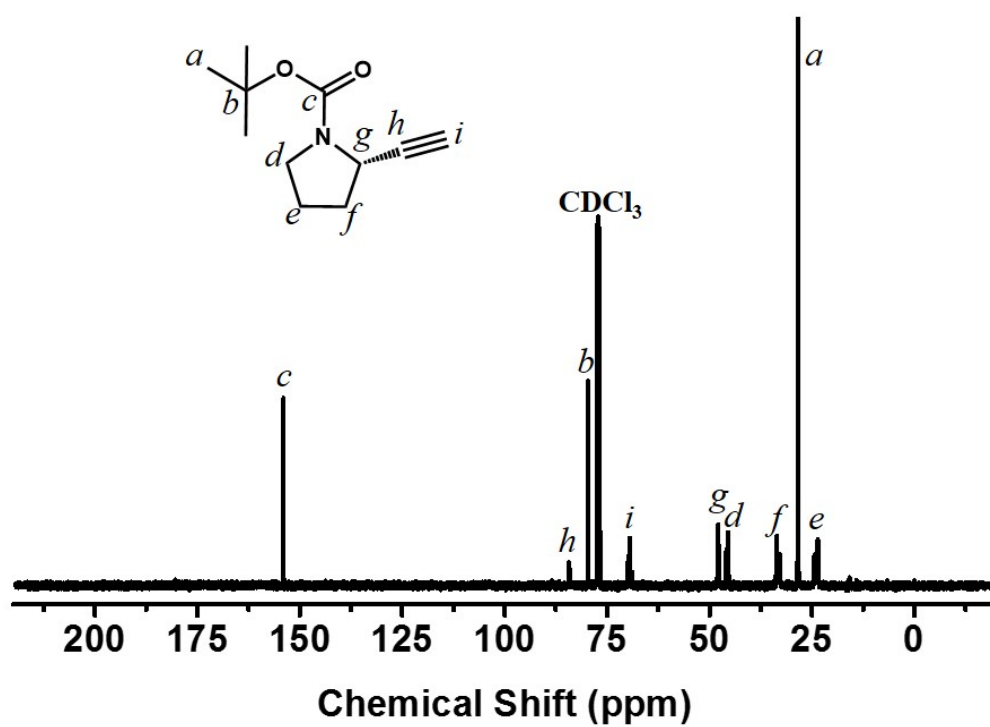


**Figure S2.**  $^{13}\text{C}$  NMR spectrum of mBoc measured in  $\text{CDCl}_3$  at room temperature.

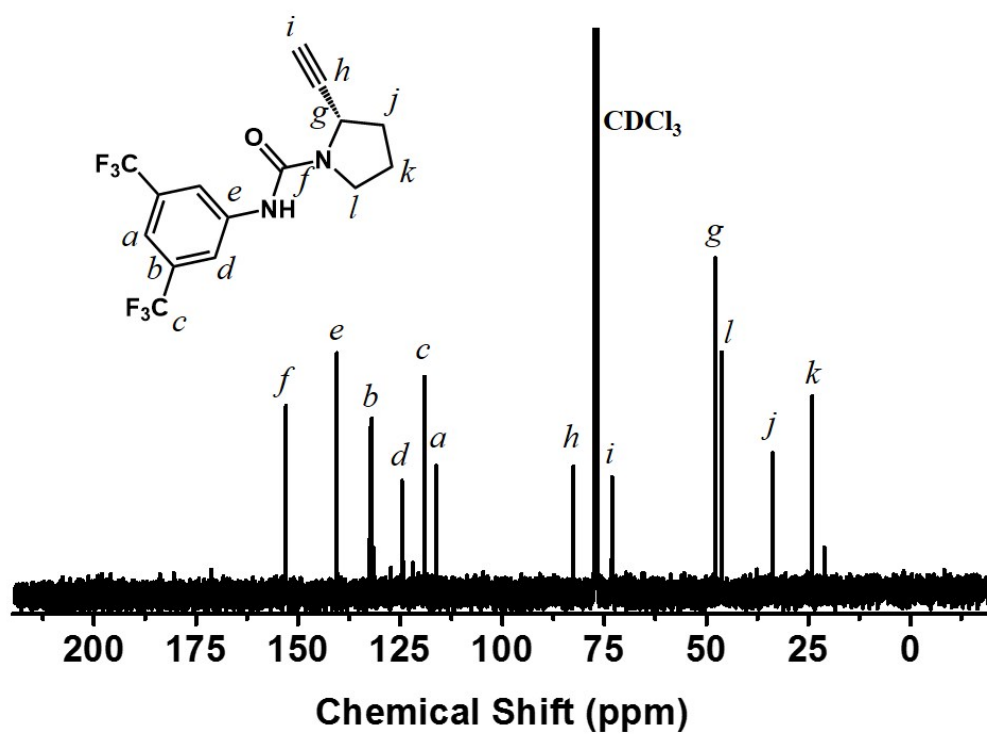


**Figure S3.**  $^{13}\text{C}$  NMR spectrum of m2CF<sub>3</sub> measured in  $\text{CDCl}_3$  at room temperature.

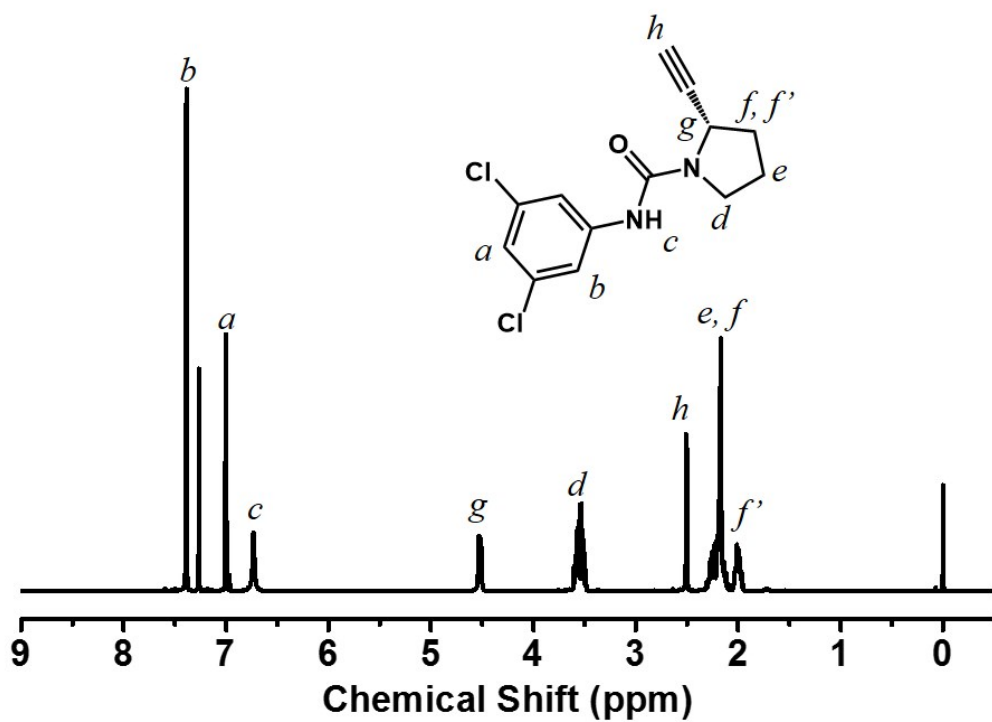


Figure S4.  $^1\text{H}$  NMR spectrum of m2Cl measured in  $\text{CDCl}_3$  at room temperature.

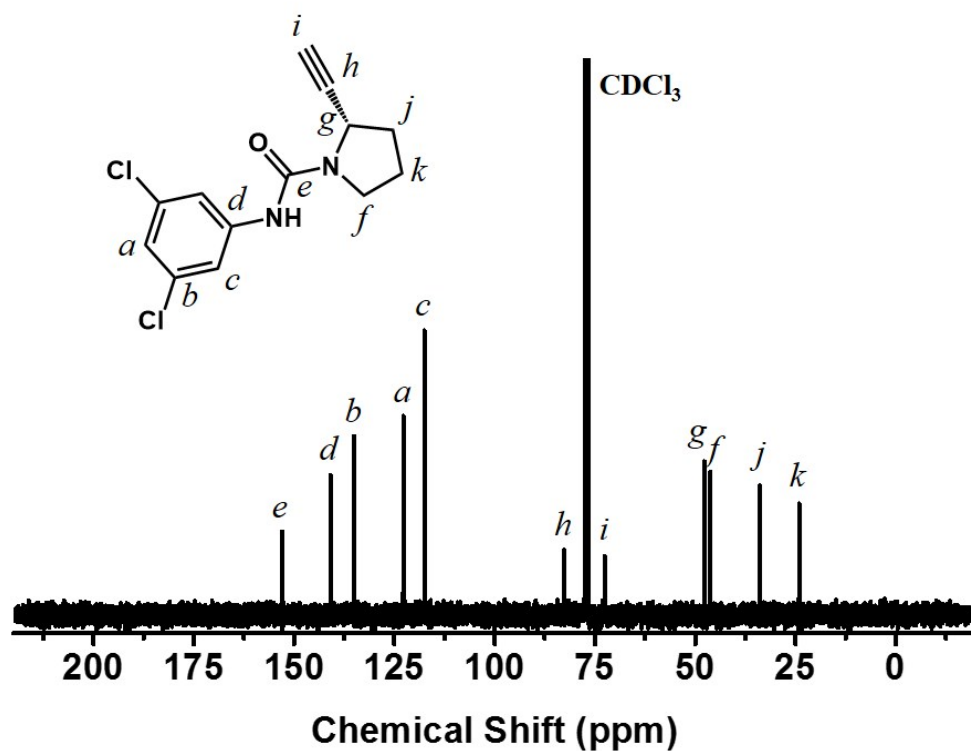


Figure S5.  $^{13}\text{C}$  NMR spectrum of m2Cl measured in  $\text{CDCl}_3$  at room temperature.

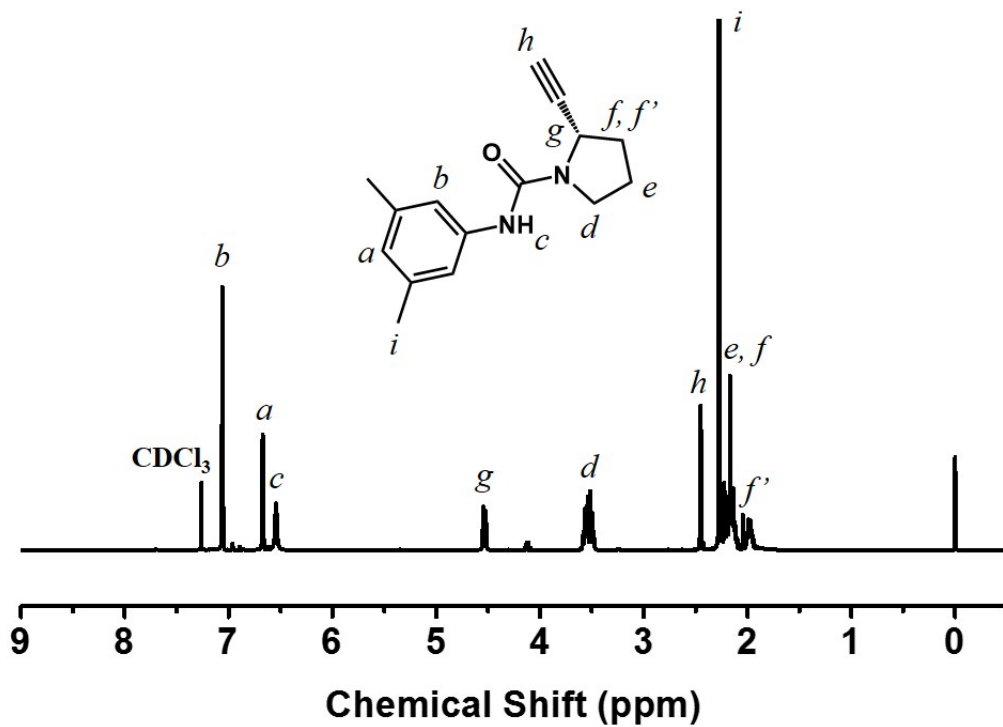


Figure S6.  $^1\text{H}$  NMR spectrum of m2Me measured in  $\text{CDCl}_3$  at room temperature.

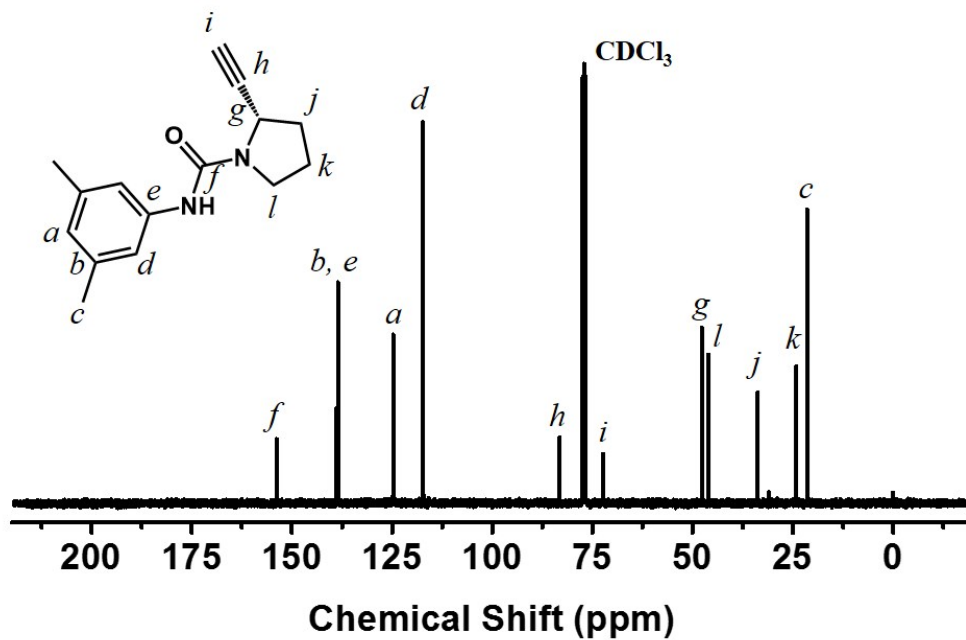
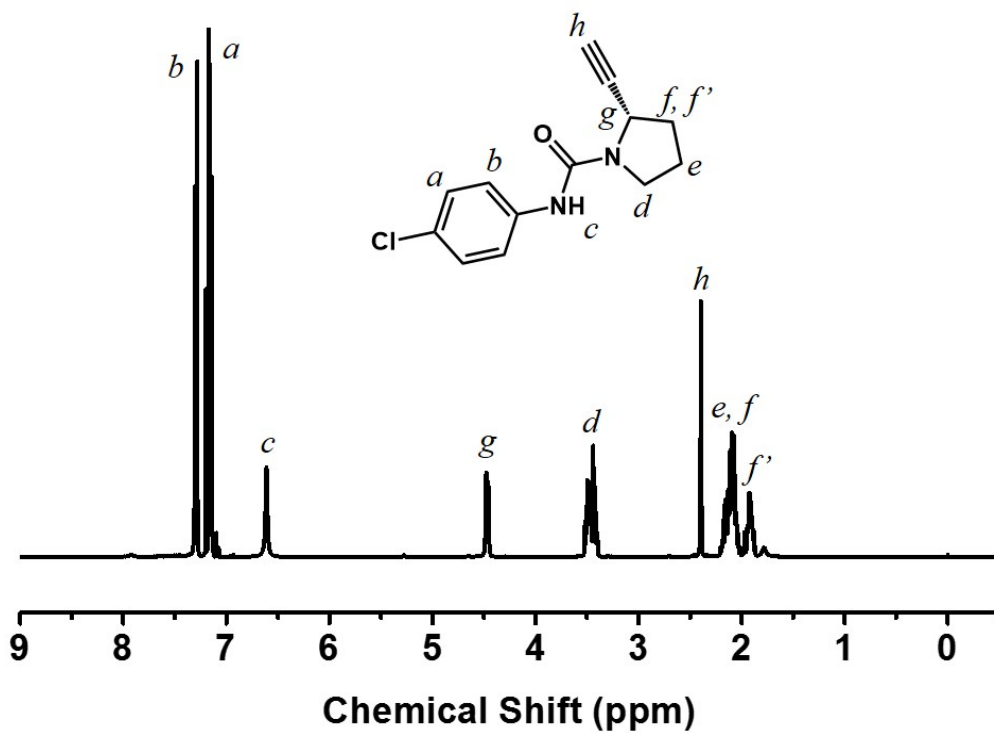
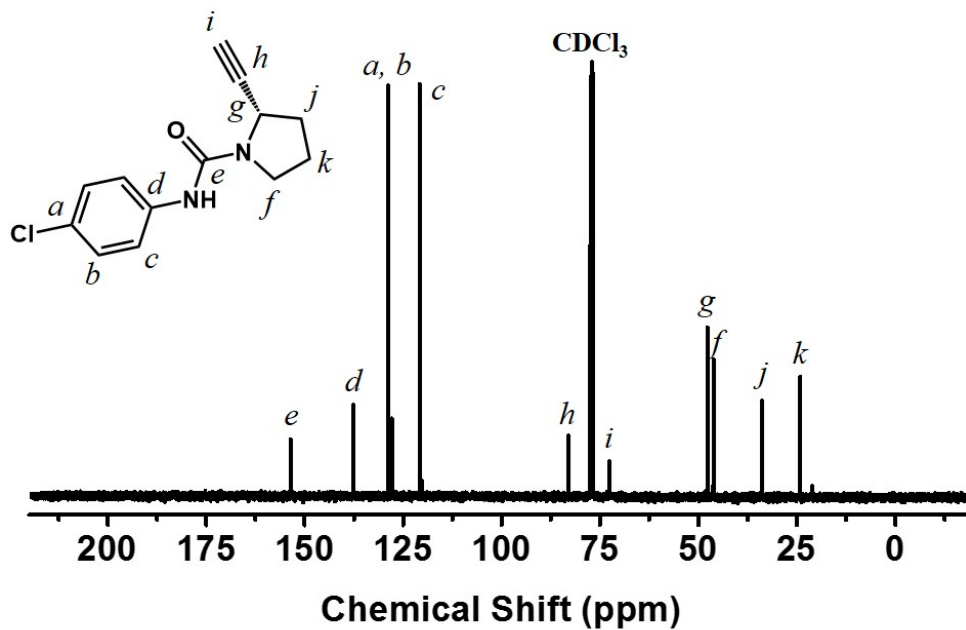


Figure S7.  $^{13}\text{C}$  NMR spectrum of m2Me measured in  $\text{CDCl}_3$  at room temperature.



**Figure S8.**  $^1\text{H}$  NMR spectrum of  $m^4\text{Cl}$  measured in  $\text{CDCl}_3$  at room temperature.



**Figure S9.**  $^{13}\text{C}$  NMR spectrum of  $m^4\text{Cl}$  measured in  $\text{CDCl}_3$  at room temperature.

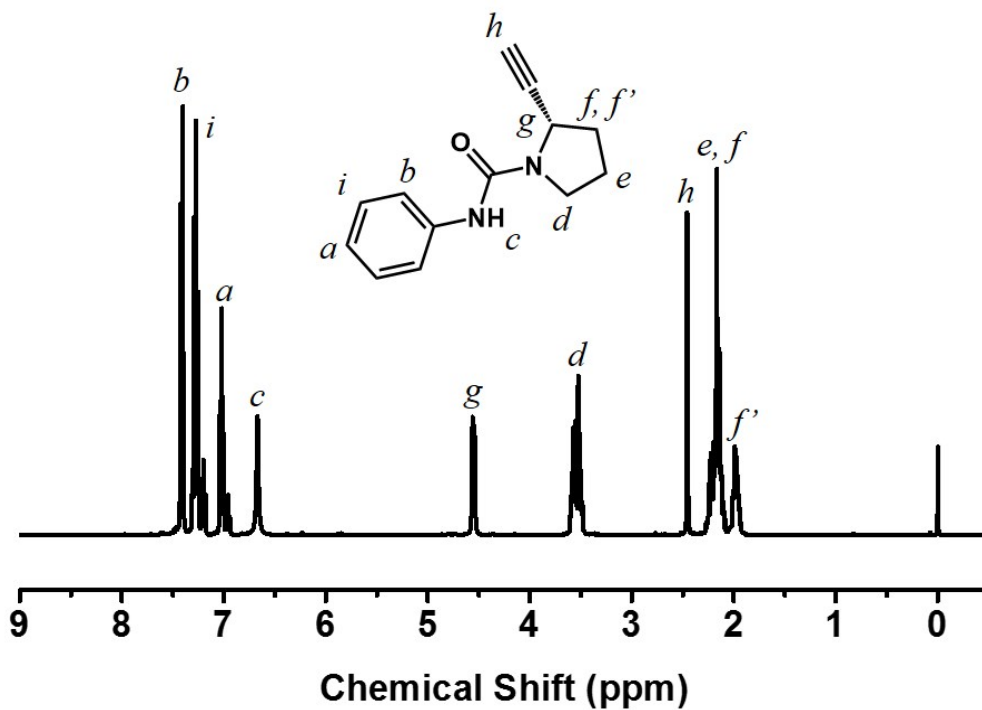


Figure S10.  $^1\text{H}$  NMR spectrum of mPh measured in  $\text{CDCl}_3$  at room temperature.

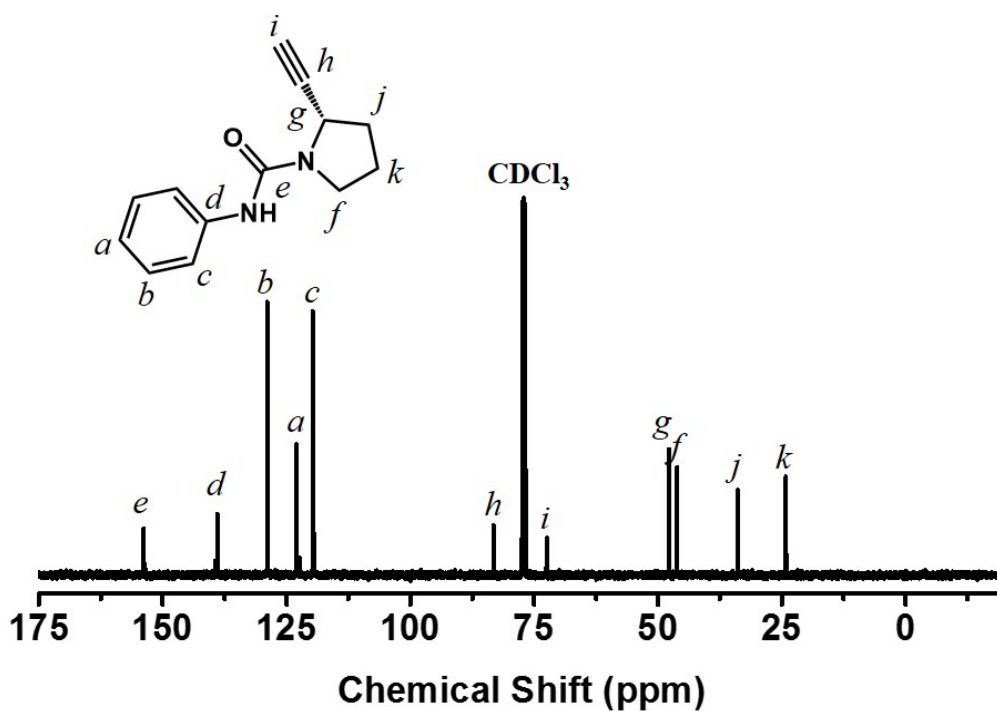


Figure S11.  $^{13}\text{C}$  NMR spectrum of mPh measured in  $\text{CDCl}_3$  at room temperature.

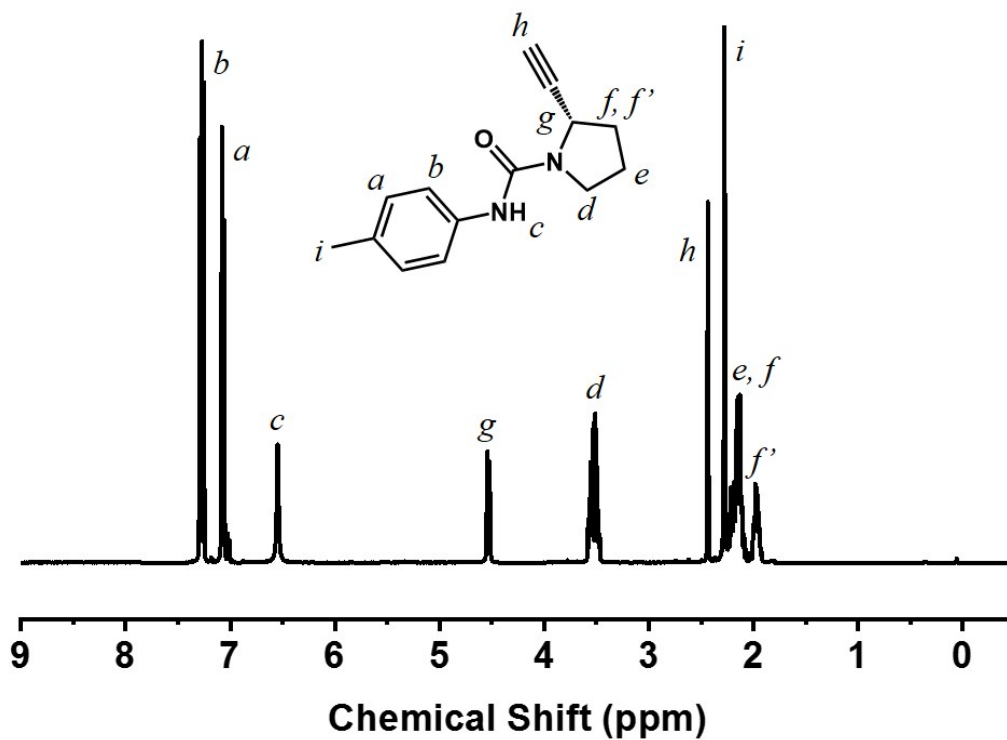


Figure S12.  $^1\text{H}$  NMR spectrum of  $m^4\text{Me}$  measured in  $\text{CDCl}_3$  at room temperature.

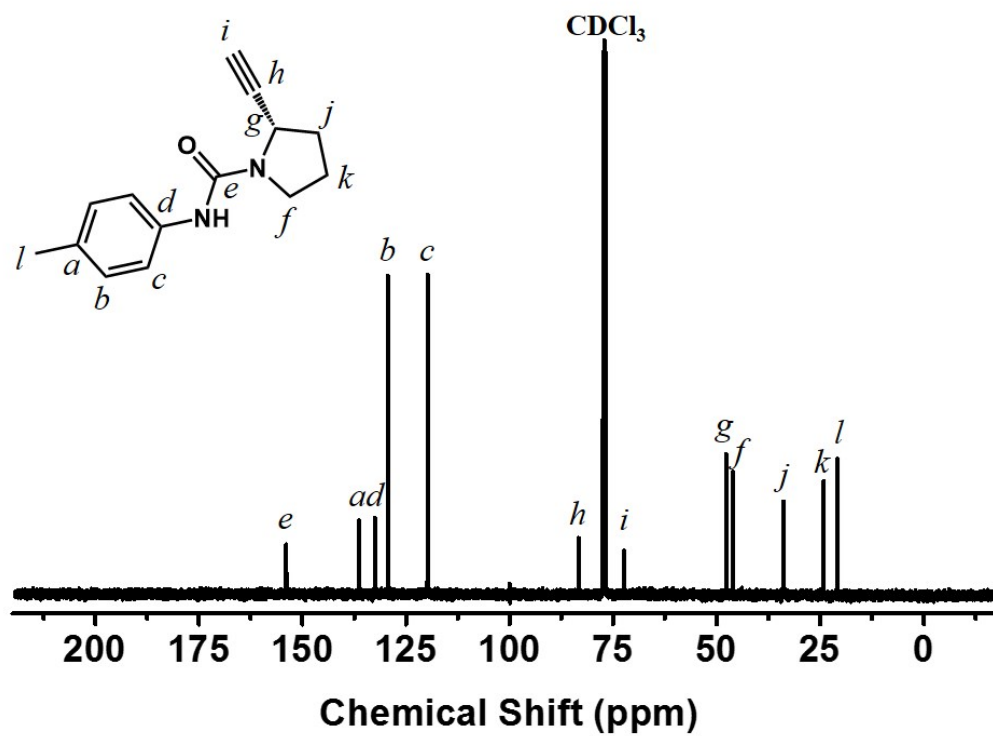


Figure S13.  $^{13}\text{C}$  NMR spectrum of  $m^4\text{Me}$  measured in  $\text{CDCl}_3$  at room temperature.

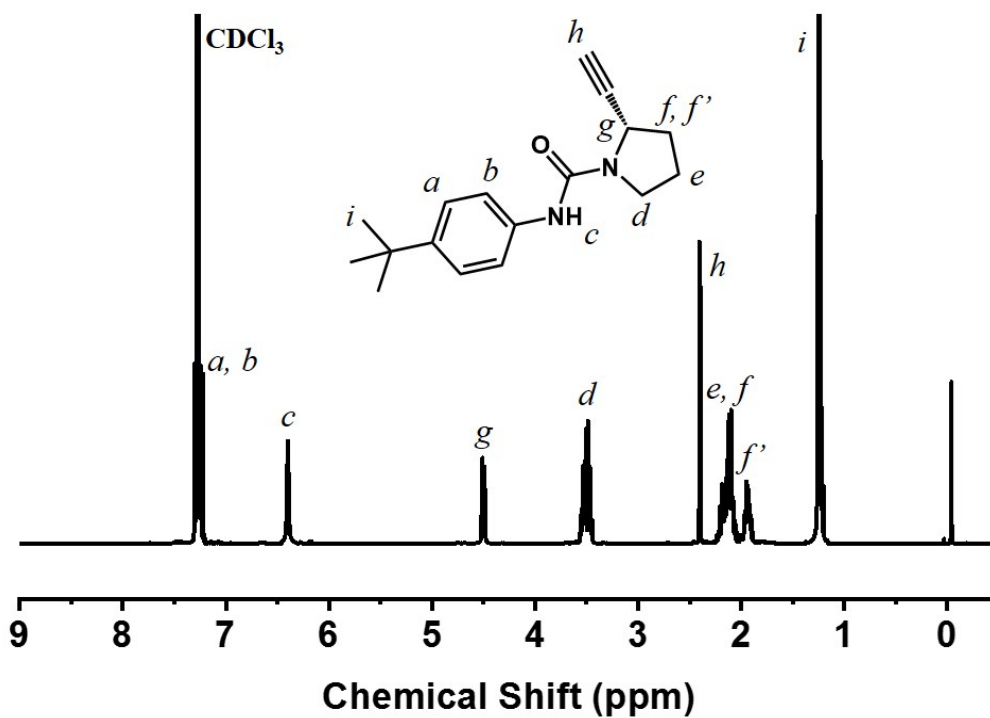


Figure S14.  $^1\text{H}$  NMR spectrum of  $m^1\text{Bu}$  measured in  $\text{CDCl}_3$  at room temperature.

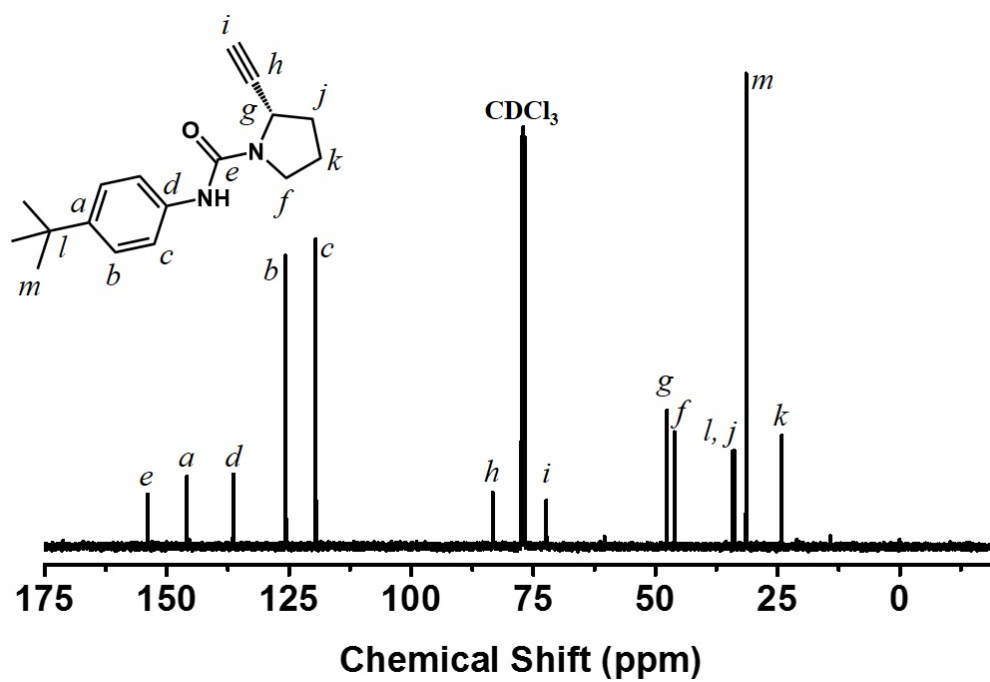


Figure S15.  $^{13}\text{C}$  NMR spectrum of  $m^1\text{Bu}$  measured in  $\text{CDCl}_3$  at room temperature.

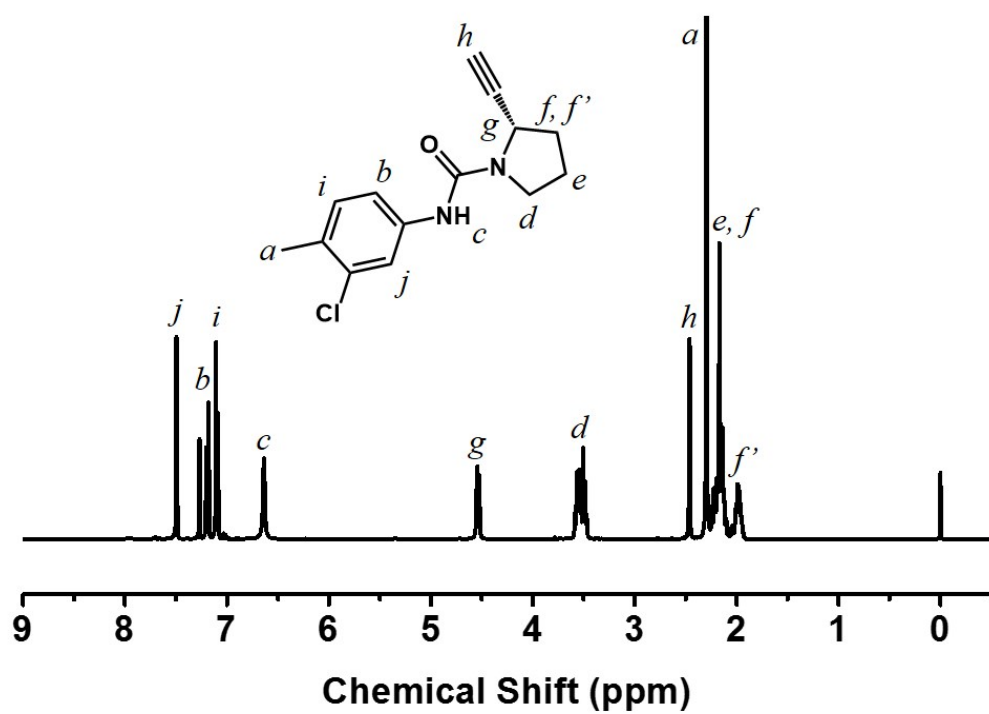


Figure S16.  $^1\text{H}$  NMR spectrum of  $m^3\text{Cl}^4\text{Me}$  measured in  $\text{CDCl}_3$  at room temperature.

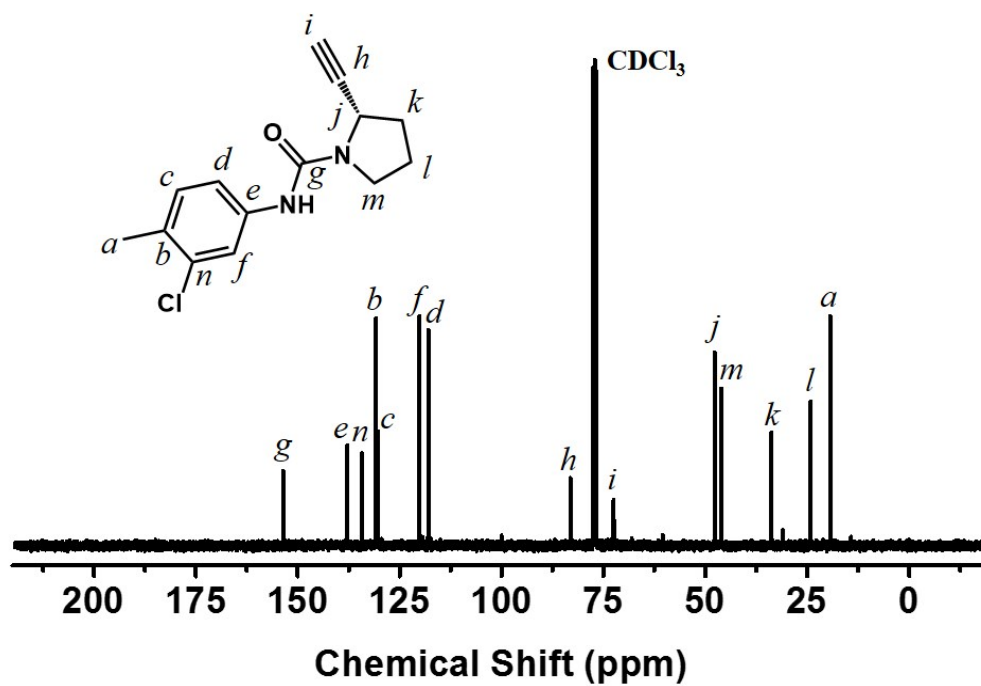


Figure S17.  $^{13}\text{C}$  NMR spectrum of  $m^3\text{Cl}^4\text{Me}$  measured in  $\text{CDCl}_3$  at room temperature.

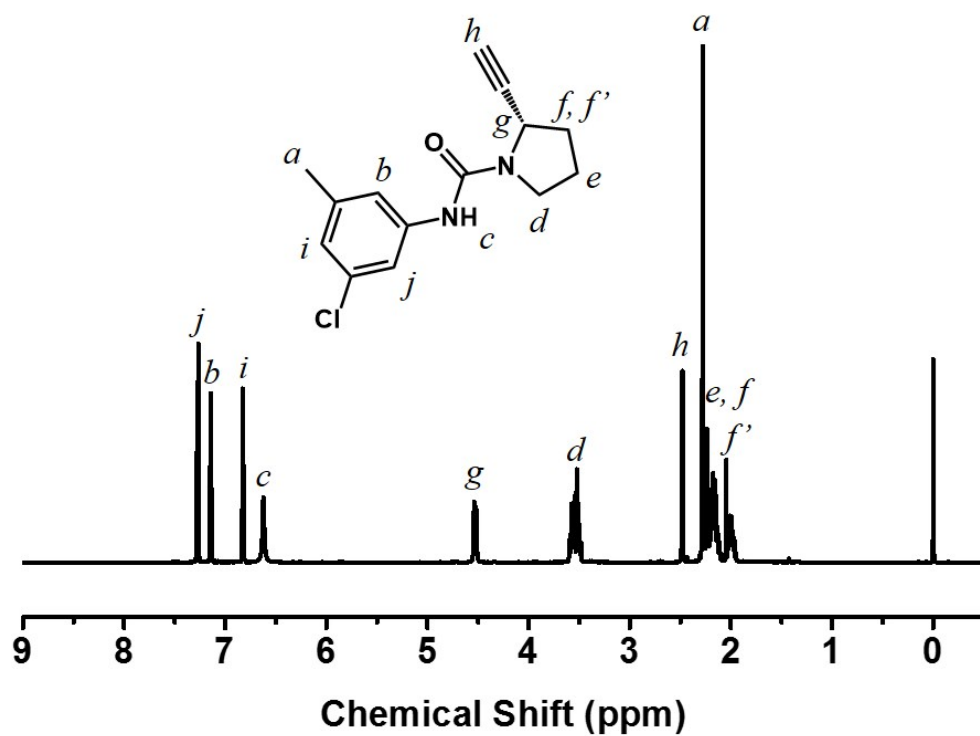


Figure S18.  $^1\text{H}$  NMR spectrum of  $m^3\text{Cl}^5\text{Me}$  measured in  $\text{CDCl}_3$  at room temperature.

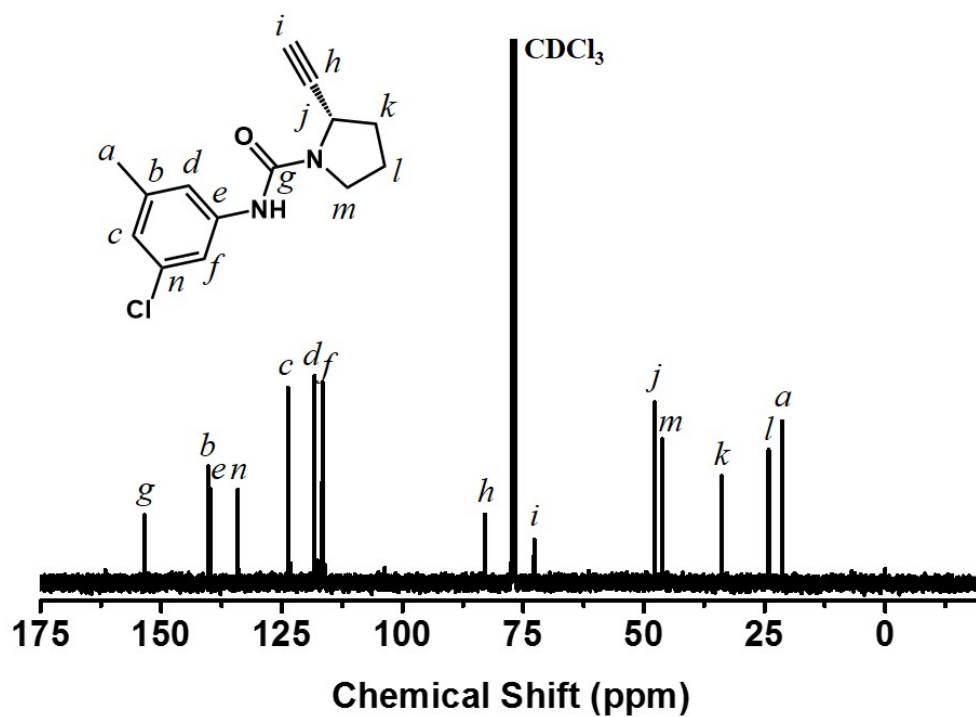


Figure S19.  $^{13}\text{C}$  NMR spectrum of  $m^3\text{Cl}^5\text{Me}$  measured in  $\text{CDCl}_3$  at room temperature.

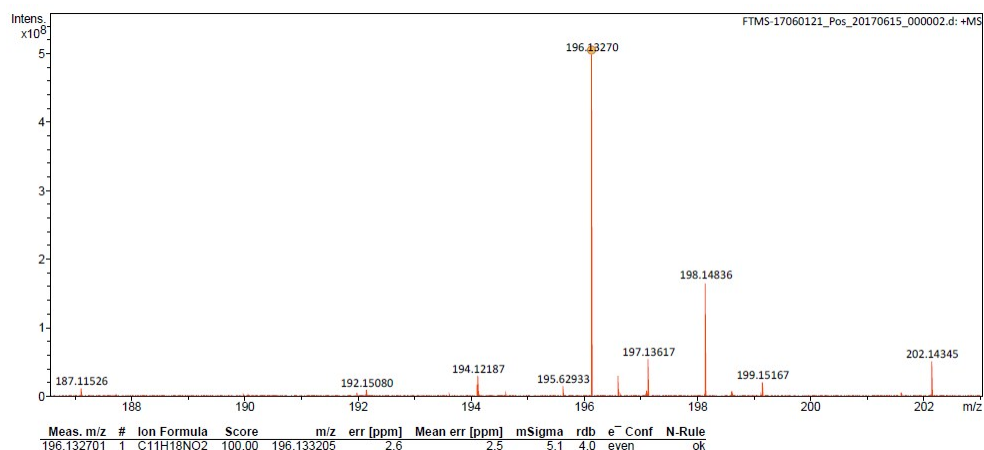


Figure S20. FTMS spectrum of mBoc.

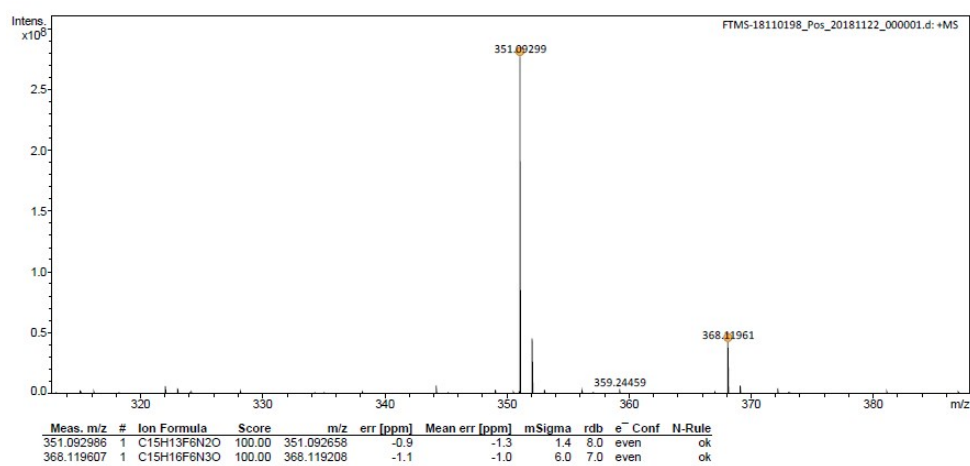


Figure S21. FTMS spectrum of m2CF<sub>3</sub>.

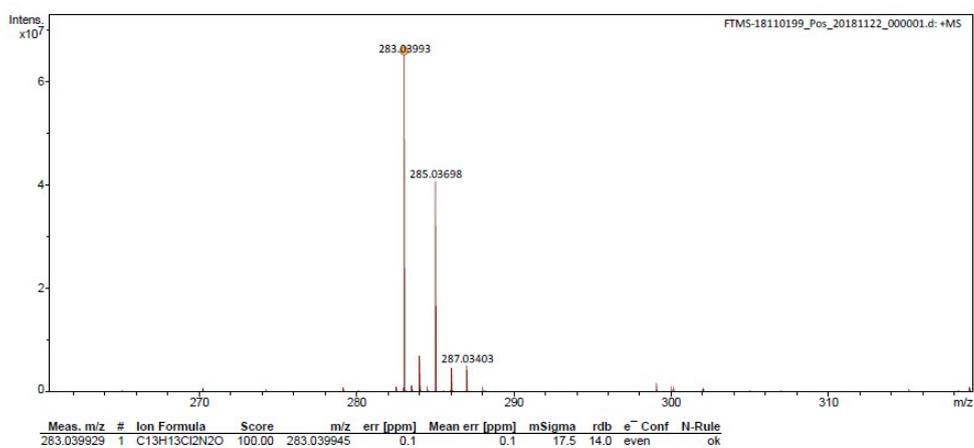


Figure S22. FTMS spectrum of m2Cl.

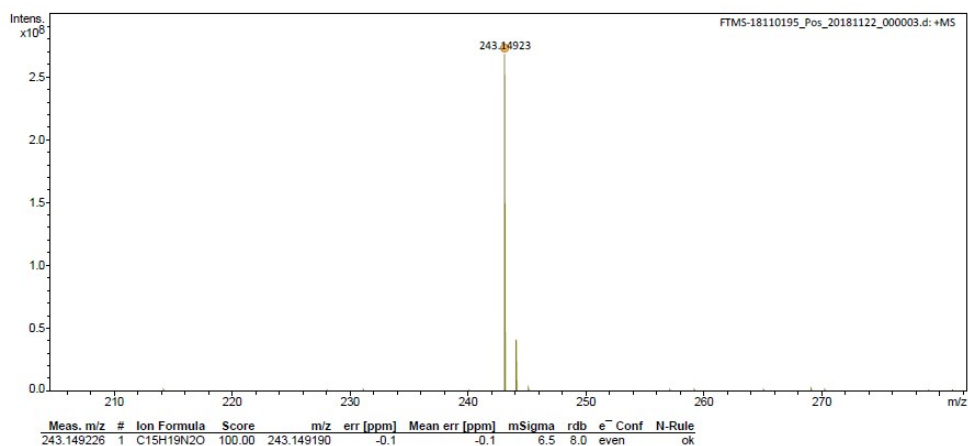


Figure S23. FTMS spectrum of m2Me.

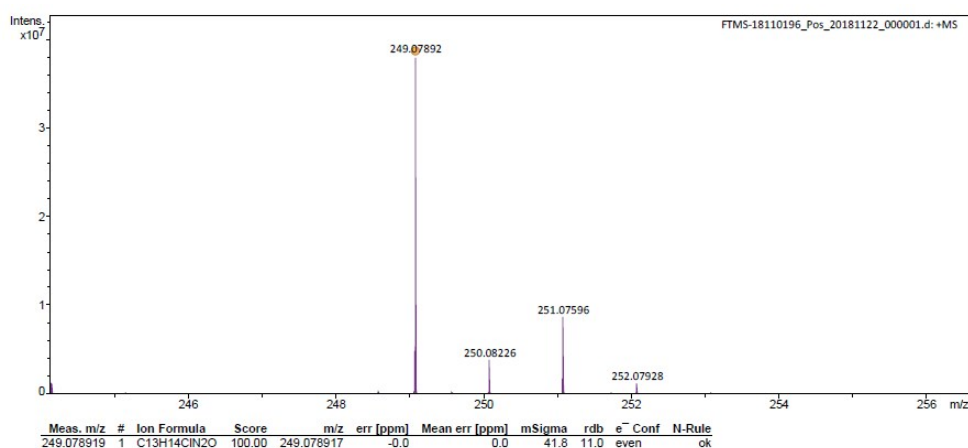


Figure S24. FTMS spectrum of m<sup>4</sup>Cl.

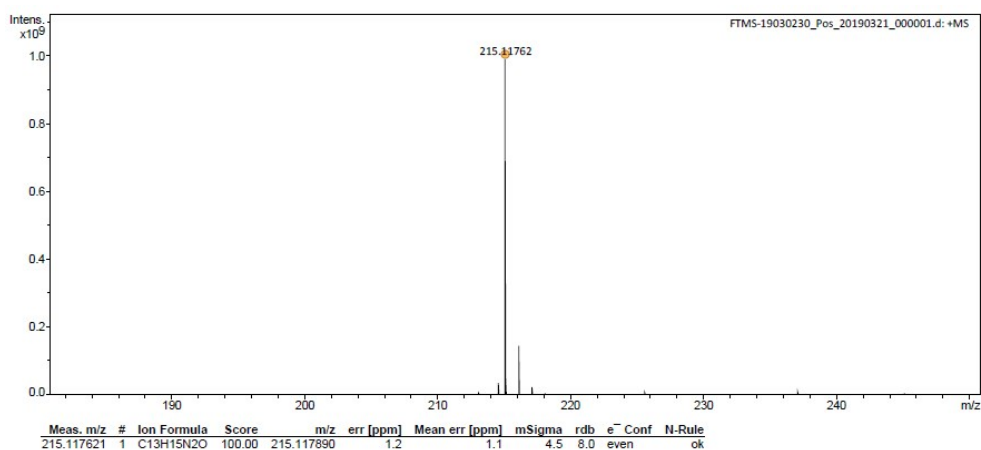


Figure S25. FTMS spectrum of mPh.

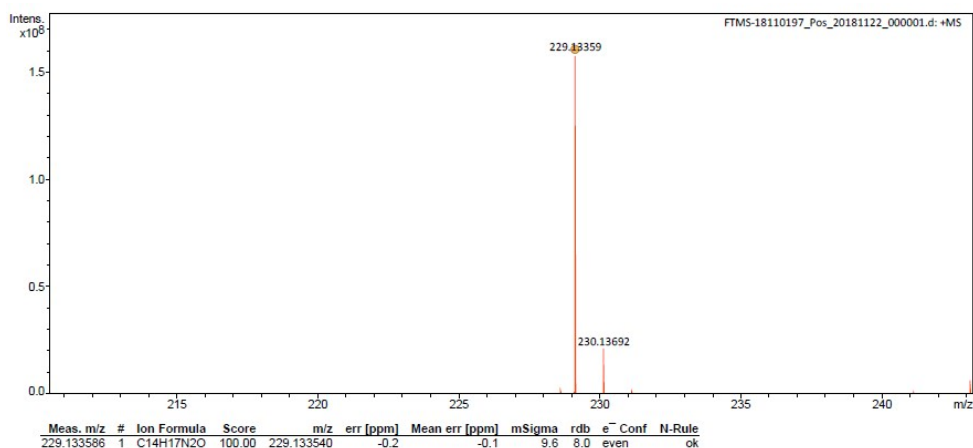


Figure S26. FTMS spectrum of m<sup>4</sup>Me.

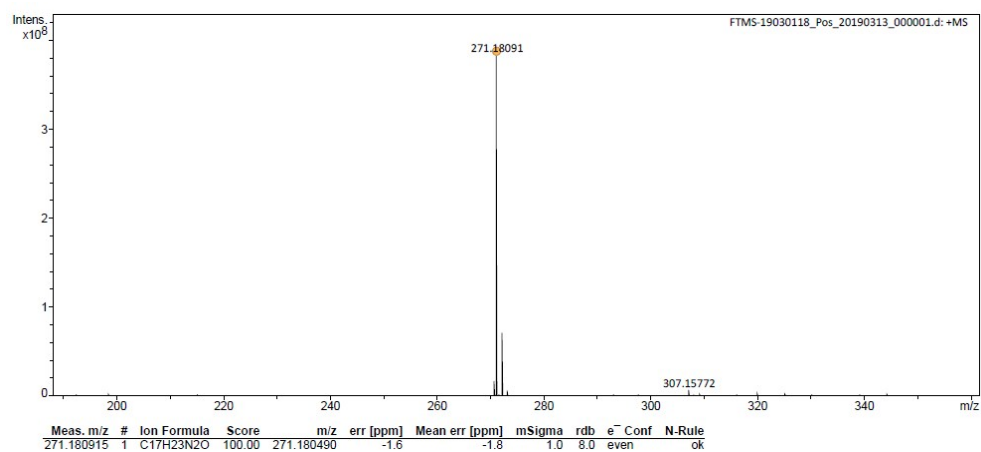


Figure S27. FTMS spectrum of m<sup>4</sup>Bu.

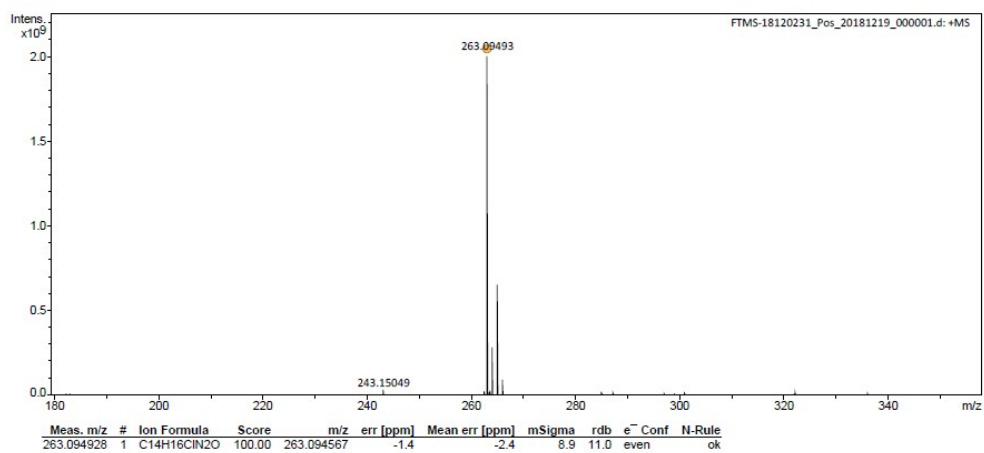


Figure S28. FTMS spectrum of m<sup>3</sup>Cl<sup>4</sup>Me.

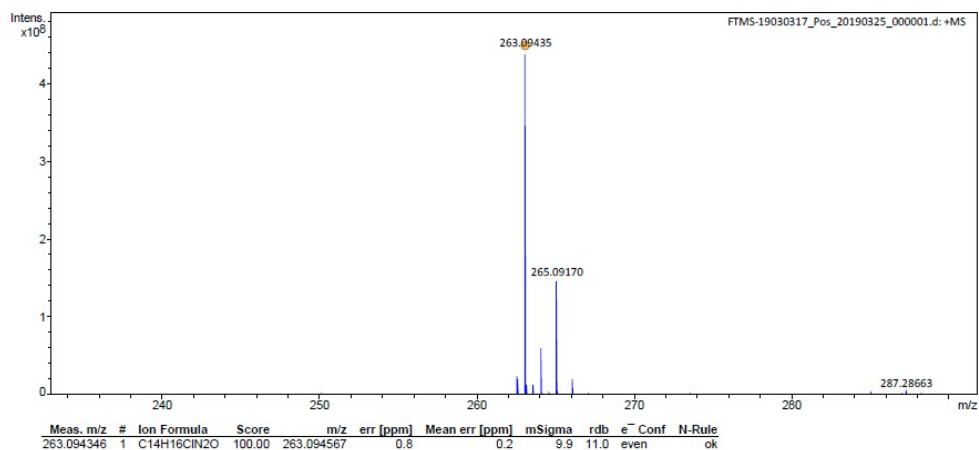


Figure S29. FTMS spectrum of  $m^3Cl^5Me$ .

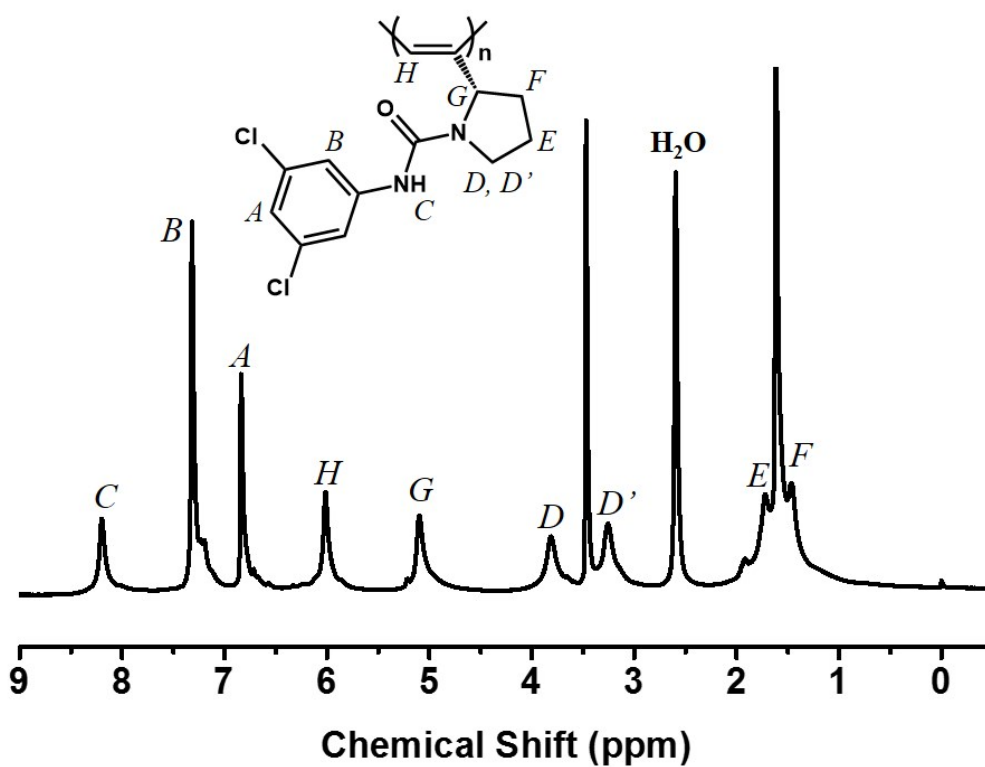
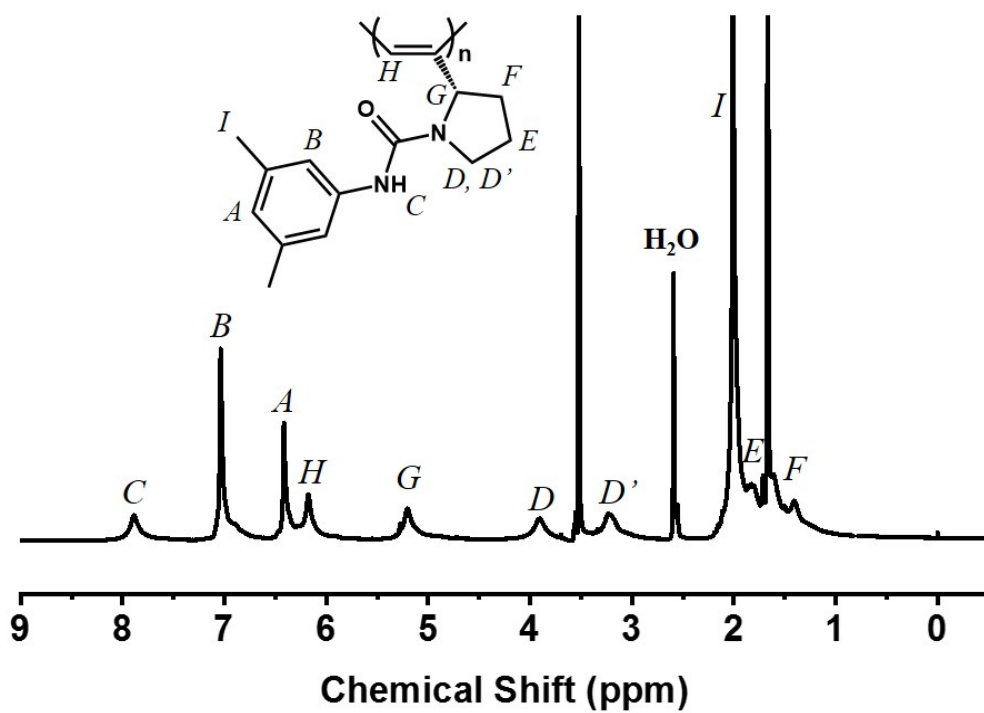
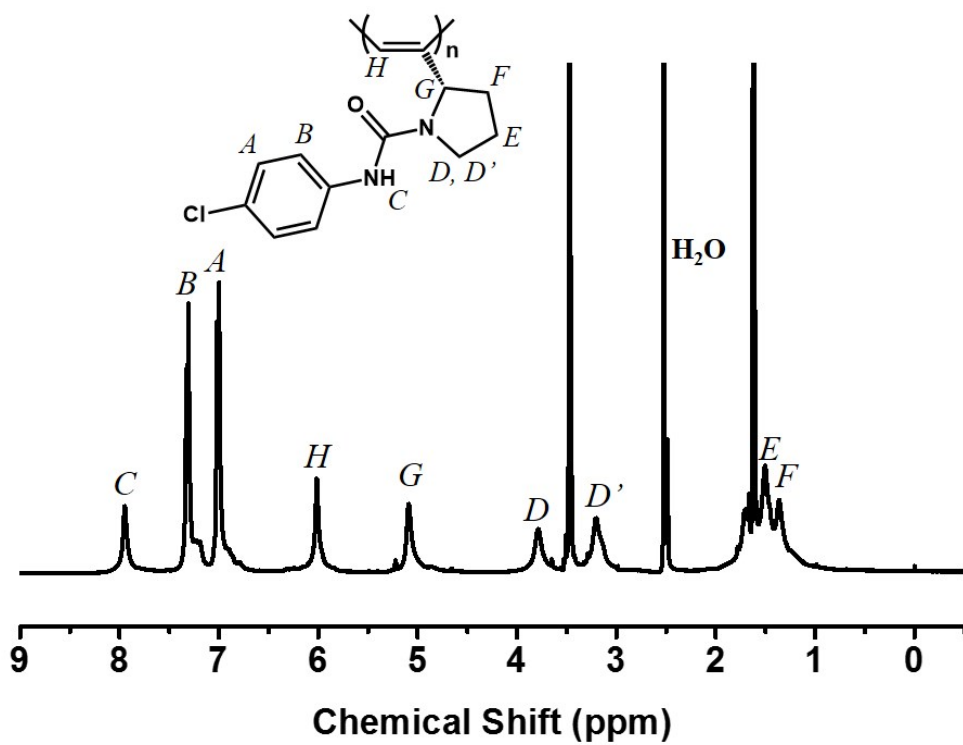


Figure S30.  $^1H$  NMR spectrum of p2Cl measured in  $d_8$ -THF at room temperature.



**Figure S31.**  $^1\text{H}$  NMR spectrum of p2Me measured in  $d_8$ -THF at room temperature.



**Figure S32.**  $^1\text{H}$  NMR spectrum of p $^4$ Cl measured in  $d_8$ -THF at room temperature.

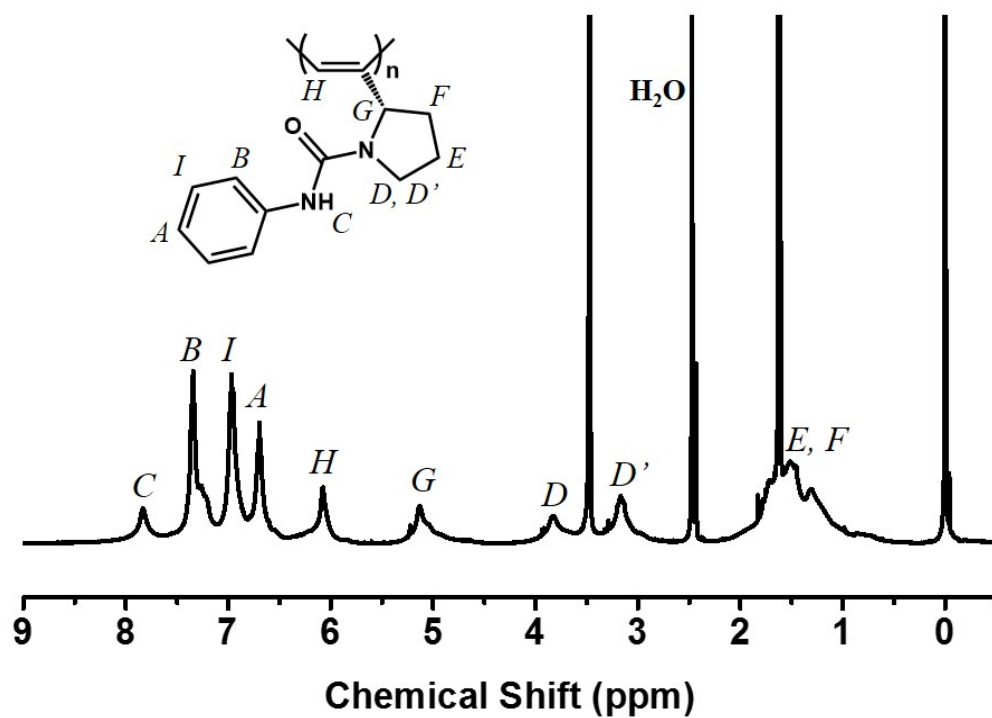


**Figure S33.**  $^1\text{H}$  NMR spectrum of pPh measured in  $d_8$ -THF at room temperature.

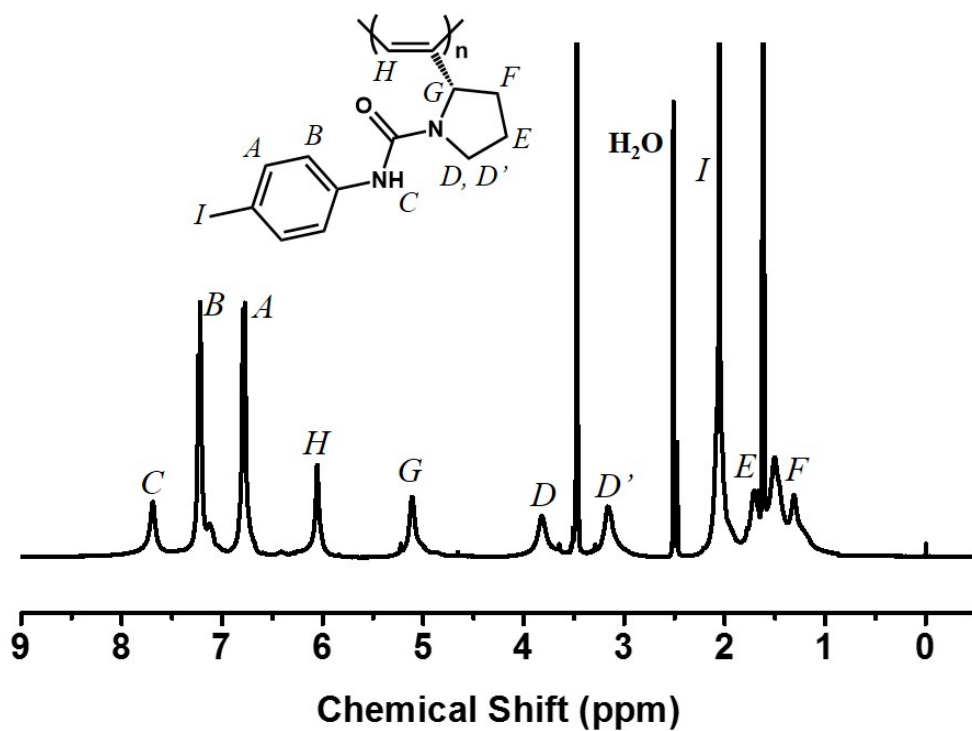


**Figure S34.**  $^1\text{H}$  NMR spectrum of p<sup>4</sup>Me measured in  $d_8$ -THF at room temperature.

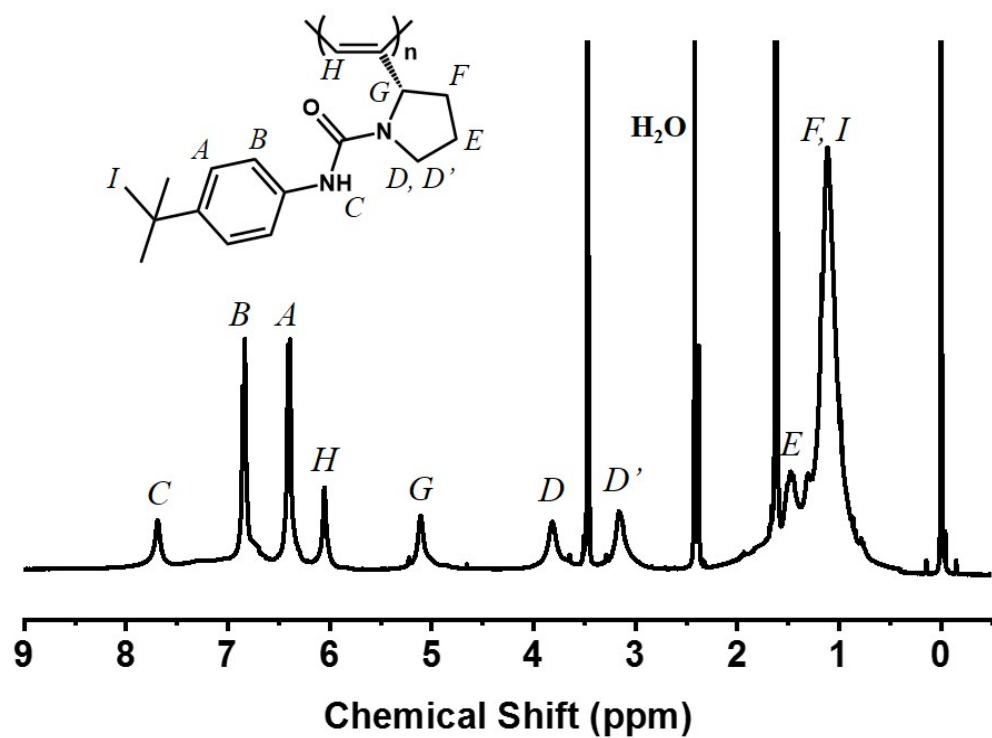


**Figure S35.** <sup>1</sup>H NMR spectrum of p<sup>4</sup>Bu measured in d<sub>8</sub>-THF at room temperature.

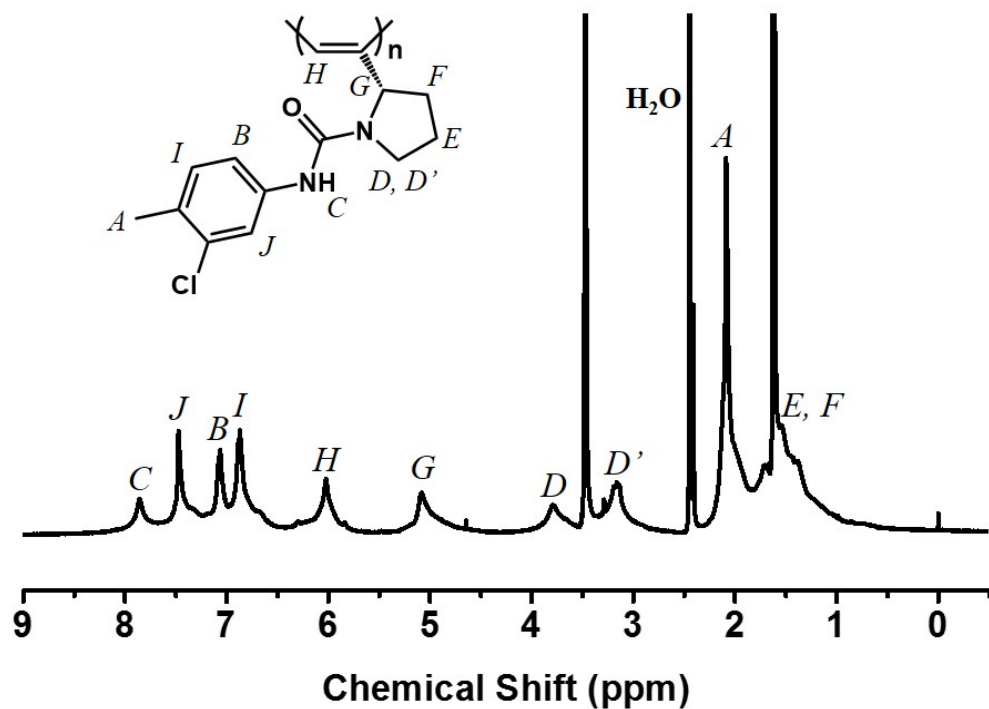


**Figure S36.** <sup>1</sup>H NMR spectrum of p<sup>3</sup>Cl<sup>4</sup>Me measured in d<sub>8</sub>-THF at room temperature.

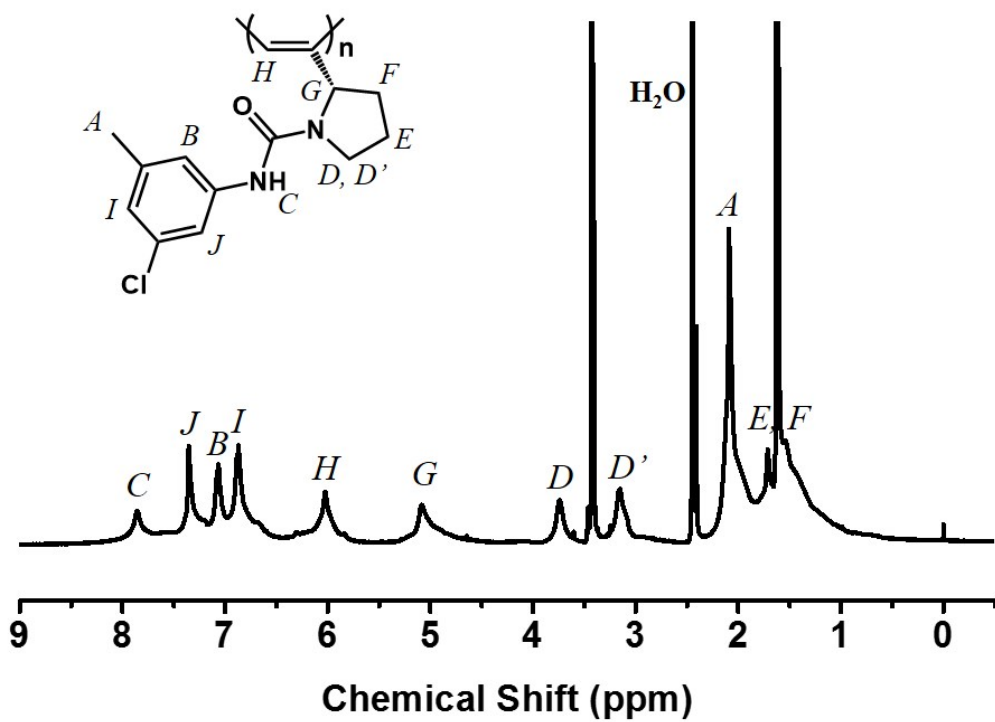


Figure S37. <sup>1</sup>H NMR spectrum of p<sup>3</sup>Cl<sup>5</sup>Me measured in d<sub>8</sub>-THF at room temperature.

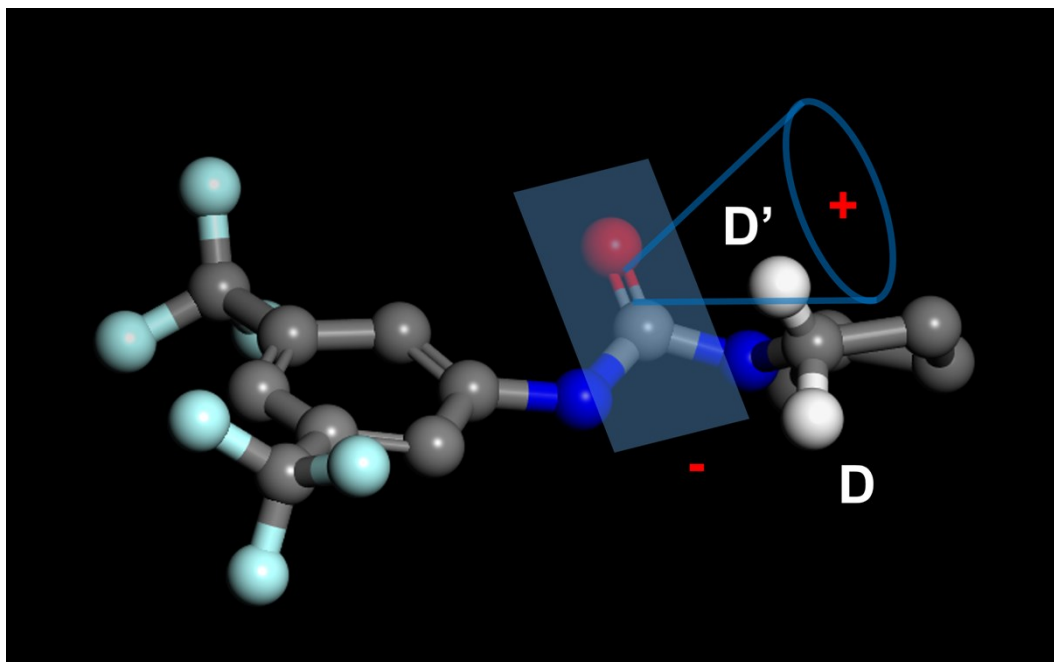
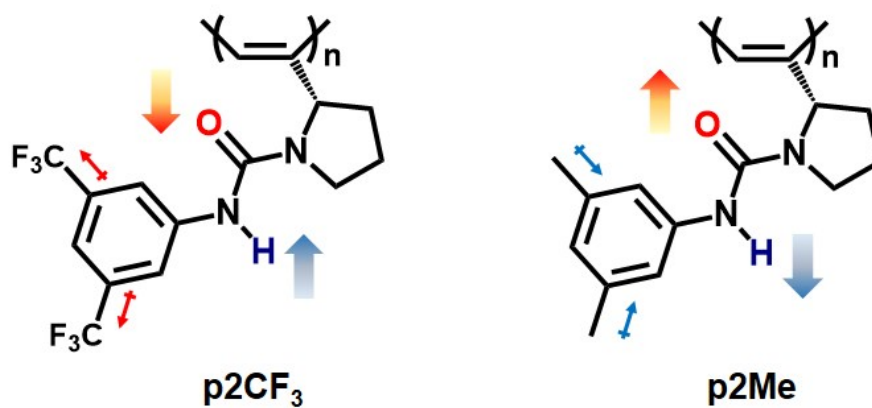
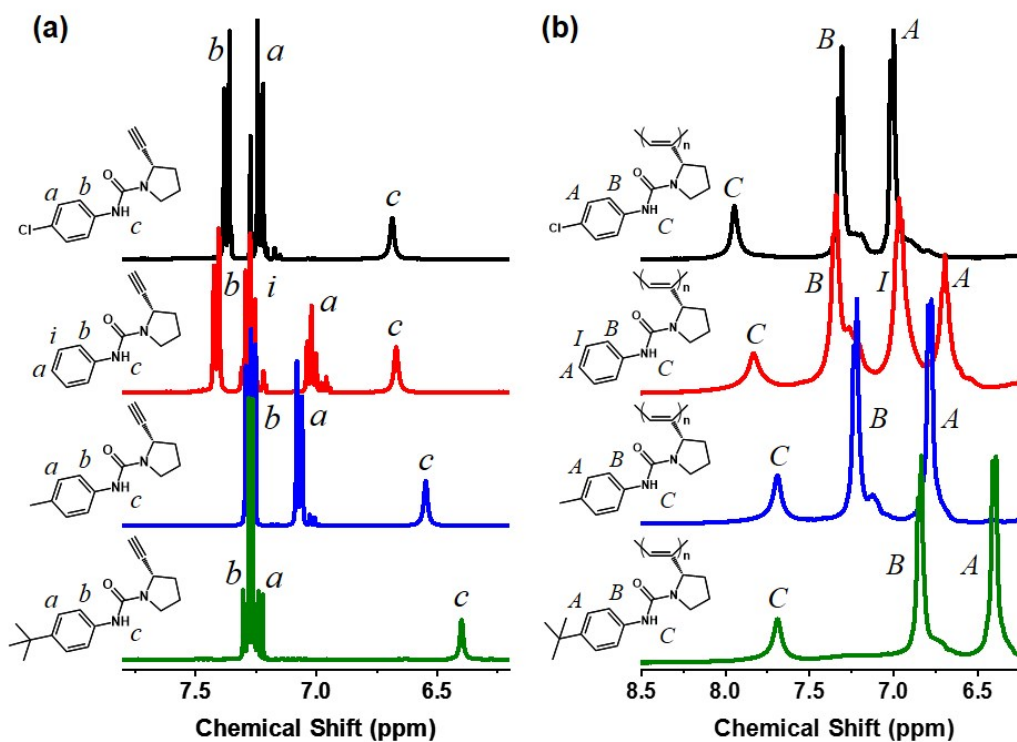


Figure S38. 3D model of pendants in p<sub>2</sub>CF<sub>3</sub>.



**Figure S39.** Schematic diagram of inductive effect on p2CF<sub>3</sub> and p2Me.



**Figure S40.** <sup>1</sup>H NMR spectra of m<sup>4</sup>Cl, mPh, m<sup>4</sup>Me and m<sup>4</sup>Bu in CDCl<sub>3</sub> (a); p<sup>4</sup>Cl, pPh, p<sup>4</sup>Me and p<sup>4</sup>Bu in d<sub>8</sub>-THF (b).

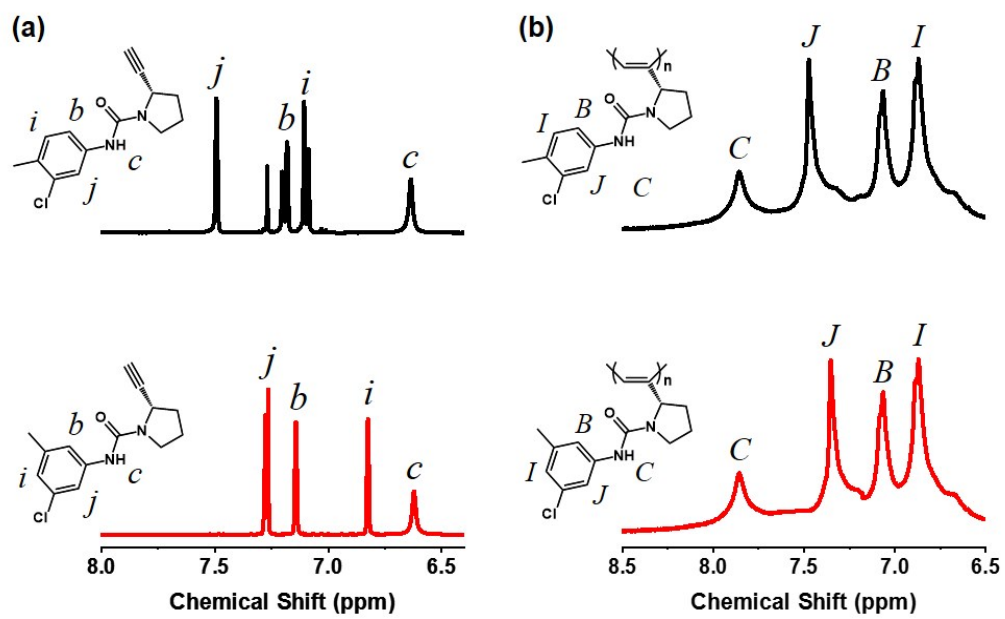


**Figure S41.** <sup>1</sup>H NMR spectra of m<sup>3</sup>Cl<sup>4</sup>Me and m<sup>3</sup>Cl<sup>5</sup>Me in CDCl<sub>3</sub> (a);  
 p<sup>3</sup>Cl<sup>4</sup>Me and p<sup>3</sup>Cl<sup>5</sup>Me in d<sub>8</sub>-THF (b).

### 3. Raman spectra of Polymers

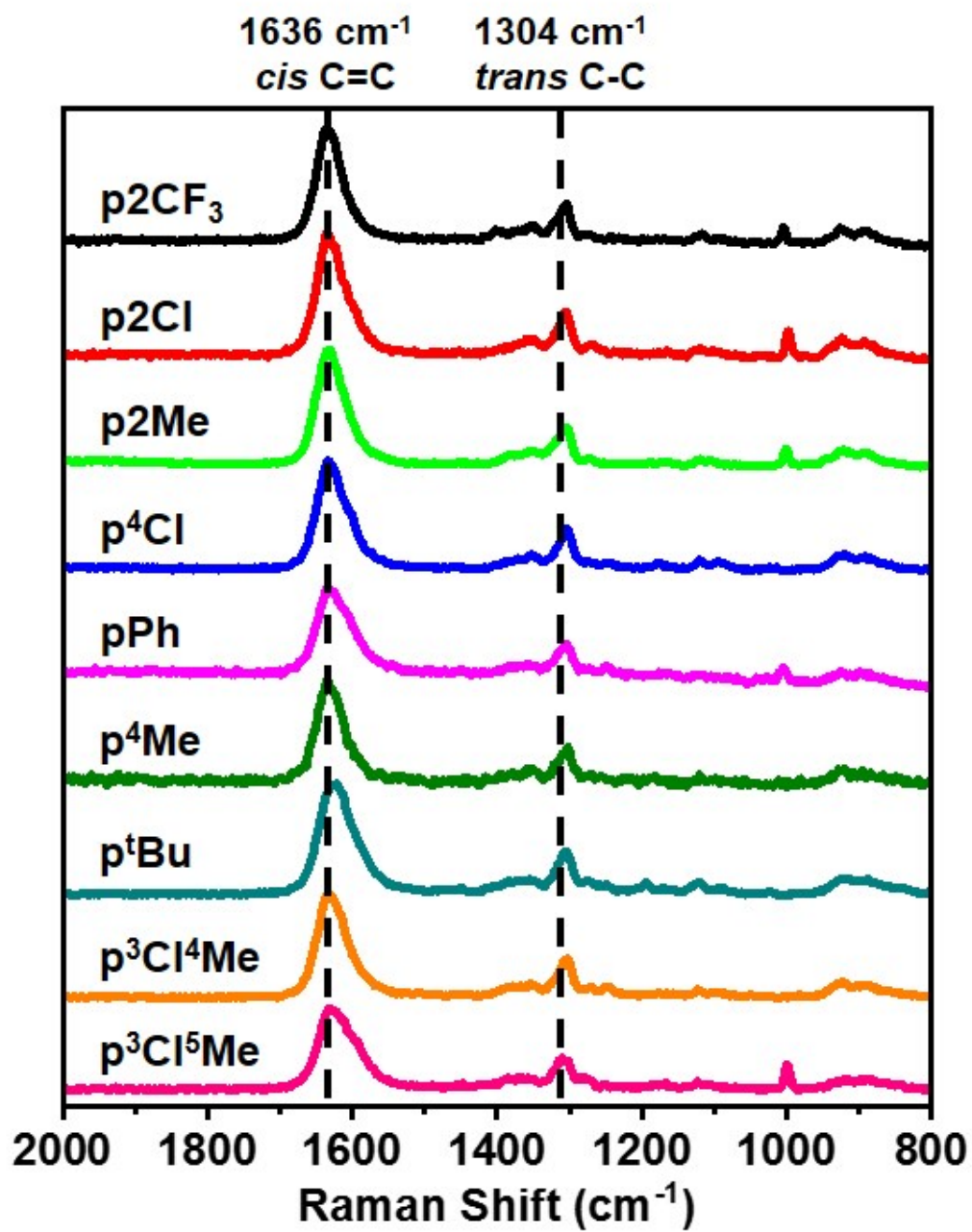


Figure S42. Raman spectra of helical polyacetylenes.

#### 4. DSC Curves of Polymers

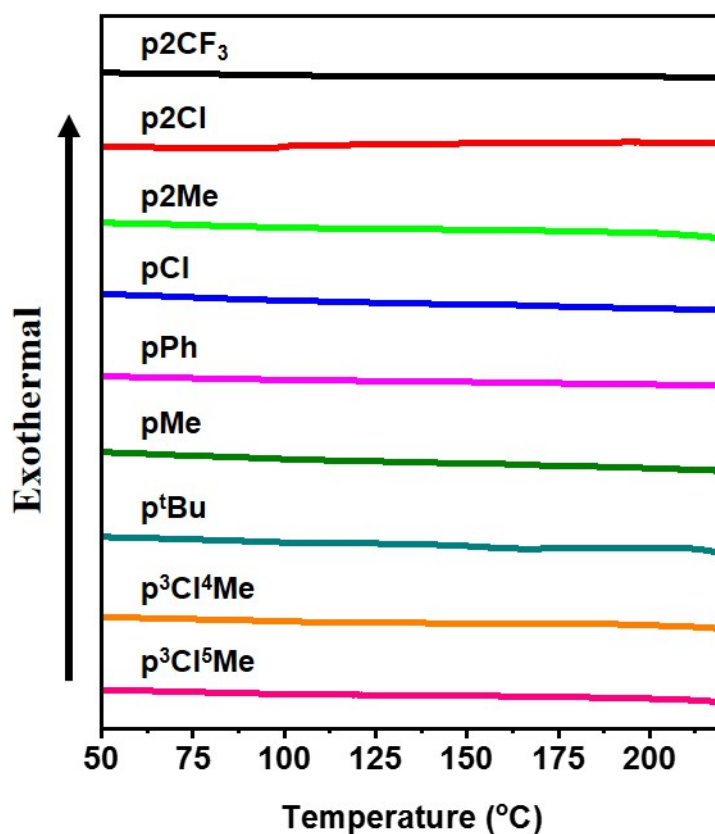


Figure S43. DSC curves of polymers recorded under nitrogen at a heating rate of 10 °C/min.

#### 5. UV-Vis Absorption and CD Spectra

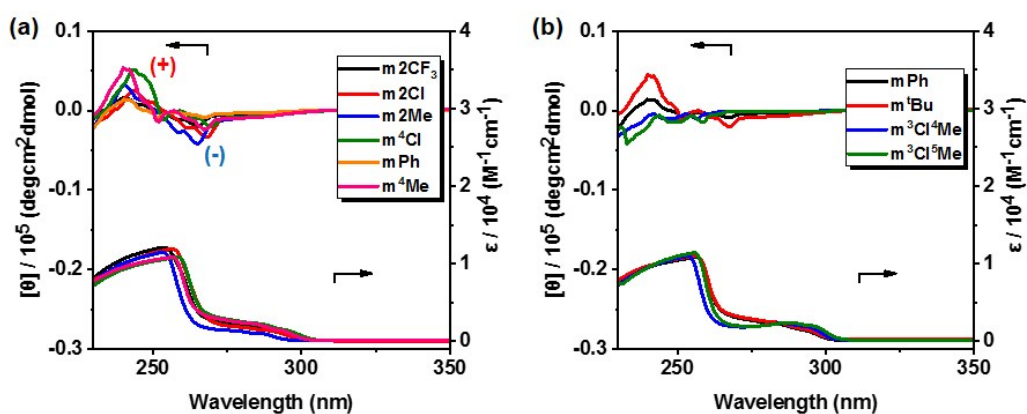
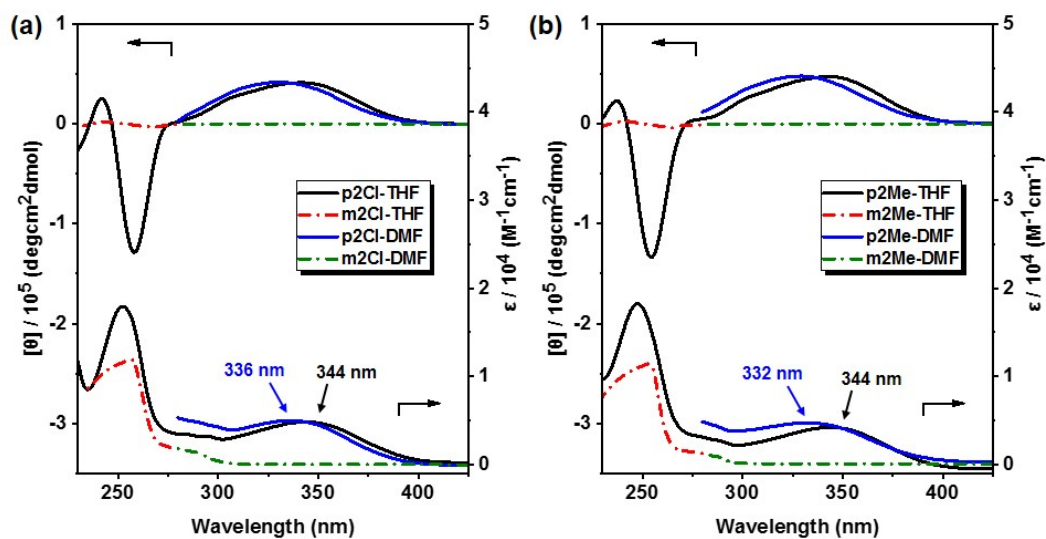
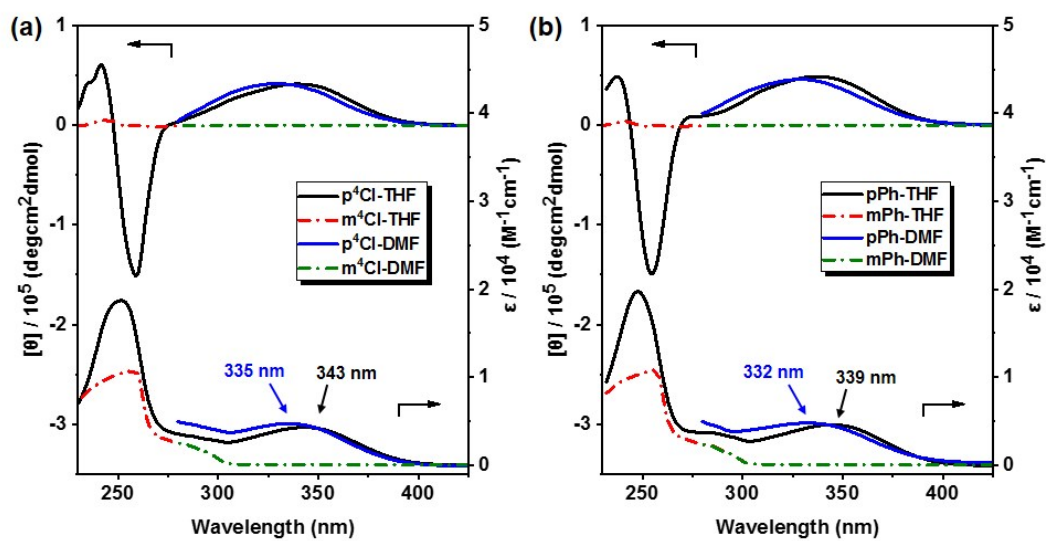


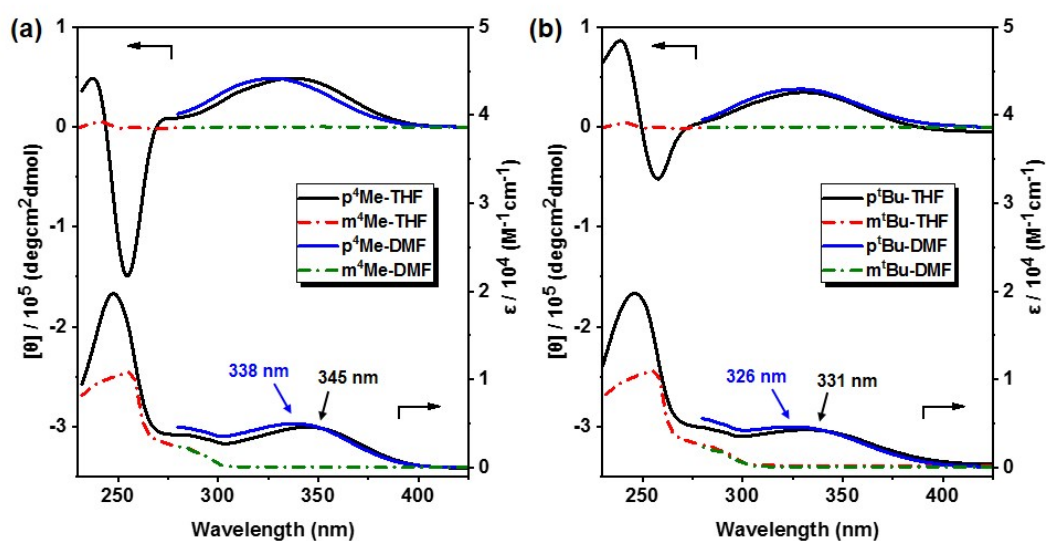
Figure S44. UV-Vis absorption and CD spectra of m2CF<sub>3</sub>, m2Cl, m2Me, m<sup>4</sup>Cl, mPh and m<sup>4</sup>Me (a); mPh, m<sup>t</sup>Bu, m<sup>3</sup>Cl<sup>4</sup>Me and m<sup>3</sup>Cl<sup>5</sup>Me (b) in THF with a concentration of 0.1 mM.



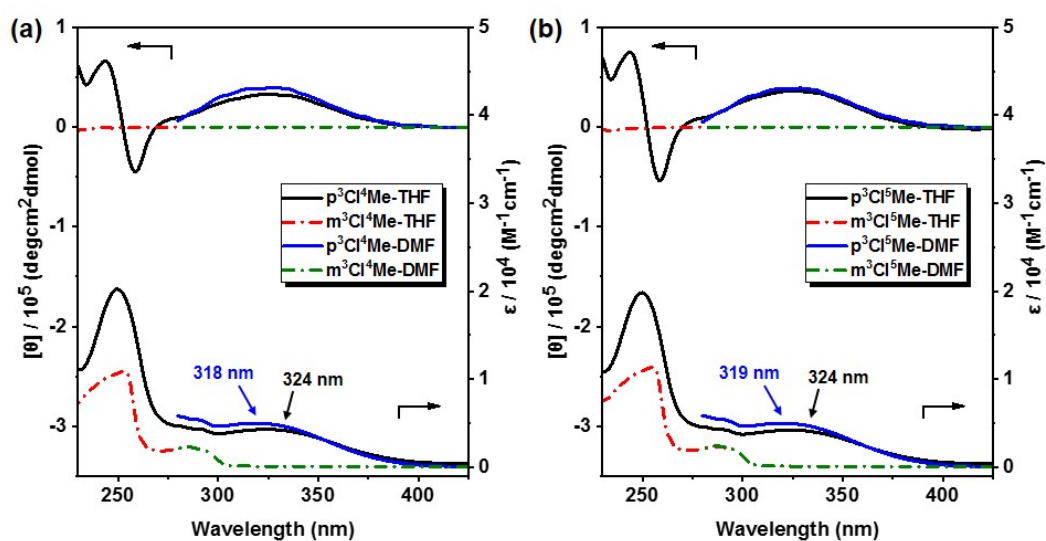
**Figure S45.** UV-Vis absorption and CD spectra of m2Cl and p2Cl (a); m2Me and p2Me (b) in THF and DMF at room temperature with a concentration of 0.1 mM.



**Figure S46.** UV-Vis absorption and CD spectra of m<sup>4</sup>Cl and p<sup>4</sup>Cl (a); mPh and pPh (b) in THF and DMF at room temperature with a concentration of 0.1 mM.



**Figure S47.** UV-Vis absorption and CD spectra of  $m^4Me$  and  $p^4Me$  (a);  $m^1Bu$  and  $p^1Bu$  (b) in THF and DMF at room temperature with a concentration of 0.1 mM.

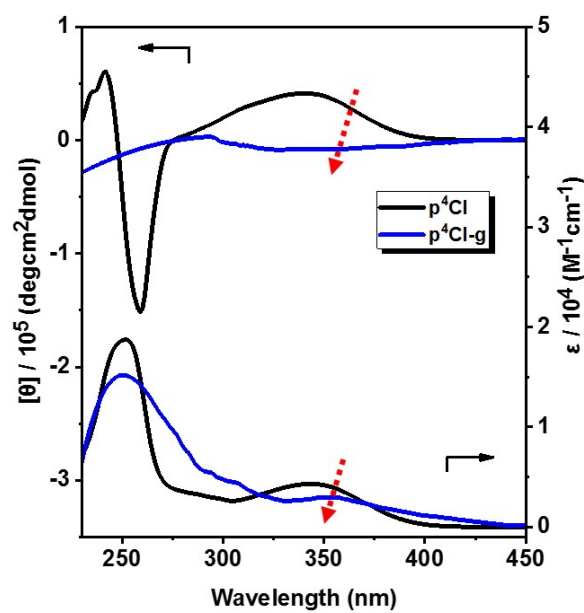


**Figure S48.** UV-Vis absorption and CD spectra of  $m^3Cl^4Me$  and  $p^3Cl^4Me$  (a);  $m^3Cl^5Me$  and  $p^3Cl^5Me$  (b) in THF and DMF at room temperature with a concentration of 0.1 mM.

**Table S1.** UV-Vis adsorption and CD results of polymers in DMF

Polymer	$\lambda_{\text{UV-Vis}}^a$ (nm)	$\lambda_{\text{CD}}^b$ (nm)	$[\theta]^c$ ( $10^4 \text{ deg}\cdot\text{cm}^2\cdot\text{dmol}$ )
p2CF <sub>3</sub>	336	326	4.44
p2Cl	336	330	4.16
p2Me	332	330	4.78
p <sup>4</sup> Cl	335	329	4.16
pPh	332	330	4.60
p <sup>4</sup> Me	338	328	4.87
p <sup>4</sup> Bu	326	329	3.80
p <sup>3</sup> Cl <sup>4</sup> Me	318	328	3.98
p <sup>3</sup> Cl <sup>5</sup> Me	319	329	3.81

<sup>a</sup> Maximum absorption wavelength of main-chain. <sup>b</sup> Wavelength of Cotton effect on main-chain. <sup>c</sup> Partial molar ellipticity of main-chain.

**Figure S49.** UV-Vis absorption and CD spectra of p<sup>4</sup>Cl and p<sup>4</sup>Cl-g in THF at room temperature with a concentration of 0.1 mM.

## 6. HPLC Results

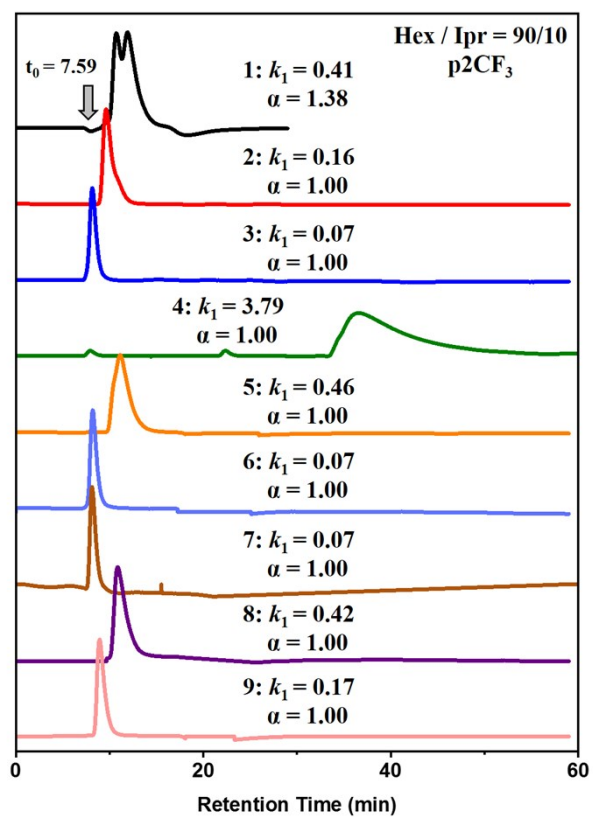


**Figure S50.** HPLC chromatograms for resolution of racemates **1-9** on p2CF<sub>3</sub>-based CSP.

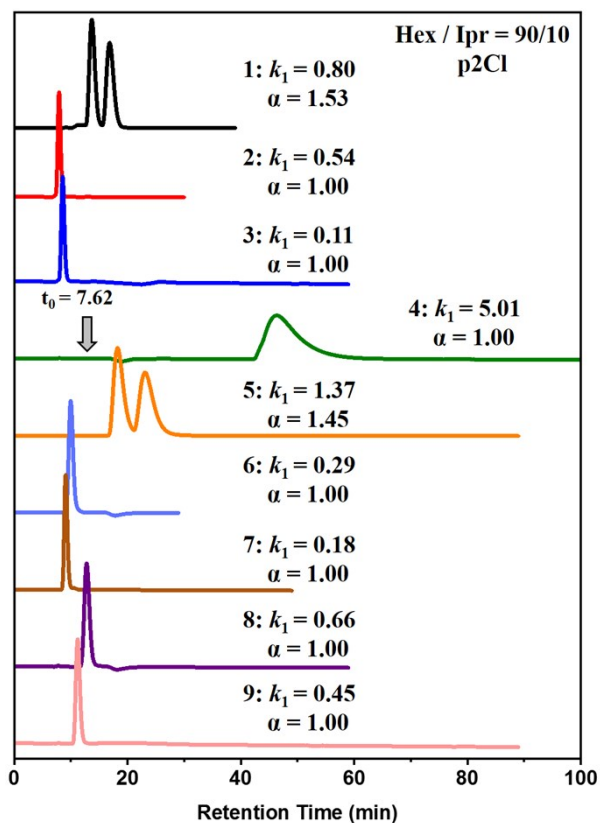


Figure S51. HPLC chromatograms for resolution of racemates 1-9 on p2Cl-based CSP.

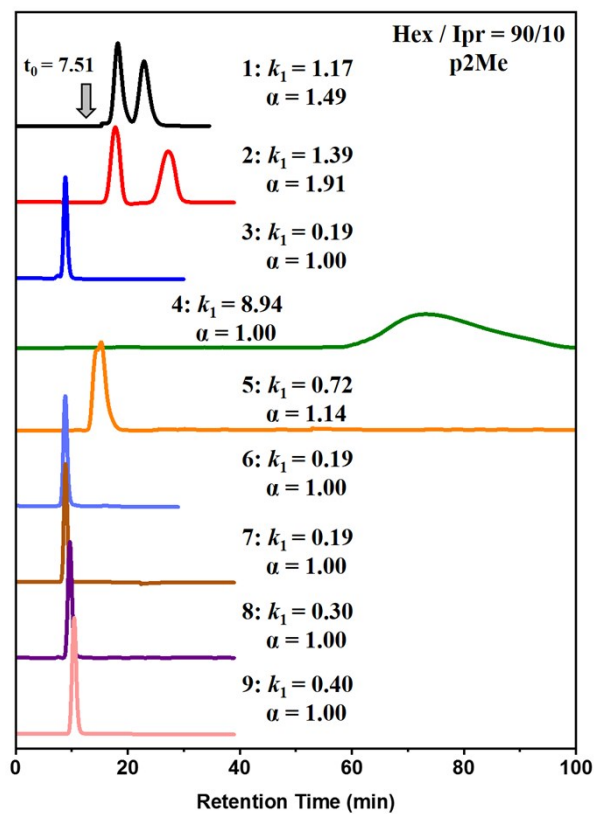


Figure S52. HPLC chromatograms for resolution of racemates 1-9 on p2Me-based CSP..

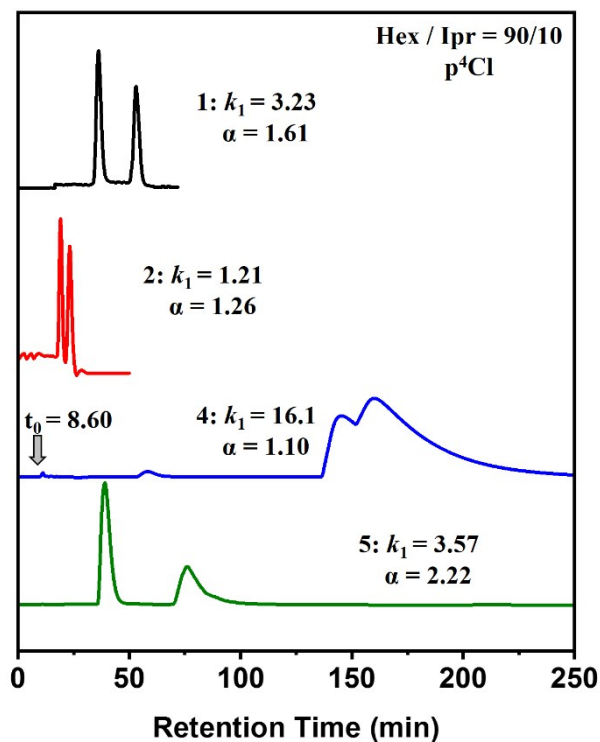


Figure S53. HPLC chromatograms for resolution of racemates 1-2 and 4-5 on p<sup>4</sup>Cl-based CSP.

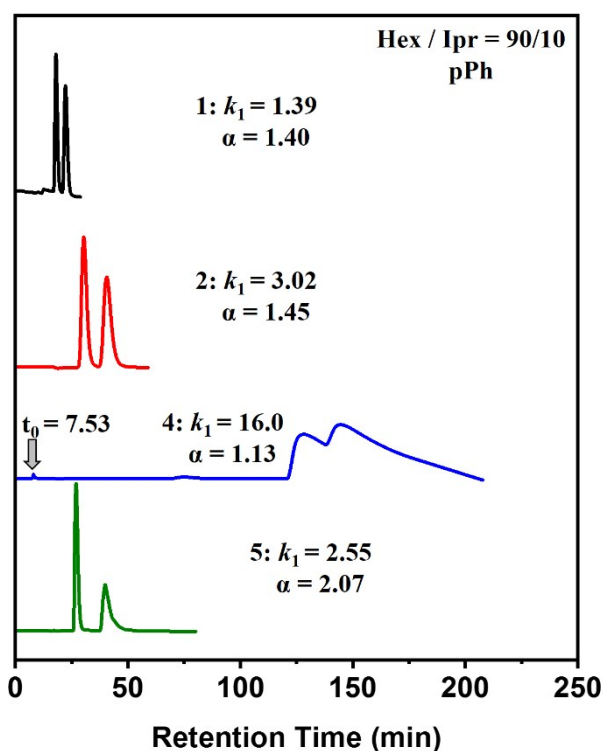
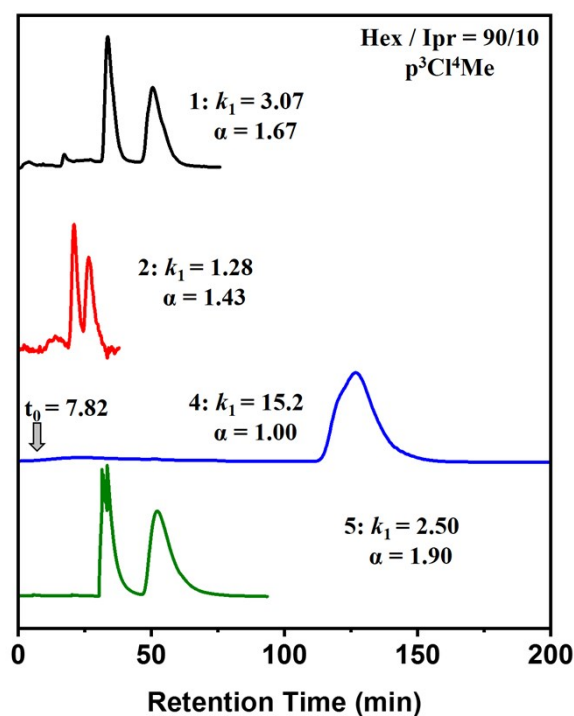


Figure S54. HPLC chromatograms for resolution of racemates 1-2 and 4-5 on pPh-based CSP.



**Figure S55.** HPLC chromatograms for resolution of racemates 1-2 and 4-5 on p<sup>3</sup>Cl<sup>4</sup>Me-based CSP.

**Table S2.** HPLC results of nine enantiomers on novel CSPs (100/0).<sup>a</sup>

Racemates	p <sup>3</sup> Cl <sup>5</sup> Me		p <sup>t</sup> Bu	
	$k_1$	$\alpha$	$k_1$	$\alpha$
1	/ <sup>b</sup>	/	/	/
2	/	/	/	/
3	7.63(+)	1.22	5.39(+)	1.22
4	/	/	0.95	1.00
5	/	/	/	/
6	4.61	1.00	3.58	1.00
7	3.67	1.00	3.88	1.00
8	7.02	1.00	8.10	1.00
9	10.9	1.00	9.52	1.00

<sup>a</sup> Column: 25 cm × 0.20 cm ID. Flow rate: 0.1 mL/min. The signs in parentheses represent the circular dichroism detection at 254 nm of the first-eluted enantiomer. Eluent: *n*-hexane/2-propanol = 100/0, v/v.

<sup>b</sup> Could not be obtained.

**Table S3.** HPLC results of nine enantiomers on novel CSPs (95/5).<sup>a</sup>

Racemates	p2CF <sub>3</sub>		p2Cl		p2Me		p <sup>4</sup> Cl	
	<i>k'</i> <sub>1</sub>	$\alpha$	<i>k'</i> <sub>1</sub>	$\alpha$	<i>k'</i> <sub>1</sub>	$\alpha$	<i>k'</i> <sub>1</sub>	$\alpha$
1	0.56(+)	1.42	1.19(+)	1.63	1.28(+)	1.51	4.26(+)	1.62
2	0.48	1.00	1.16	1.00	3.02(+)	1.91	3.57(+)	1.26
3	0.10	1.00	0.17	1.00	0.30	1.00	0.33	1.00
4 <sup>b</sup>	3.80	1.00	9.08	1.00	15.6(-)	<i>ca.</i> 1	22.3(-)	1.12
5	0.74(+)	<i>ca.</i> 1	2.61(+)	1.48	0.82(+)	1.18	4.09(+)	2.26
6	0.09	1.00	0.38(-)	<i>ca.</i> 1	0.24	1.00	0.26	1.00
7	0.07	1.00	0.20	1.00	0.22	1.00	0.30	1.00
8	0.55	1.00	0.90	1.00	0.38	1.00	0.77	1.00
9	0.20	1.00	0.59(-)	<i>ca.</i> 1	0.50	1.00	0.77	1.00

Racemates	pPh		p <sup>4</sup> Me		p <sup>3</sup> Cl <sup>4</sup> Me	
	<i>k'</i> <sub>1</sub>	$\alpha$	<i>k'</i> <sub>1</sub>	$\alpha$	<i>k'</i> <sub>1</sub>	$\alpha$
1	2.26(+)	1.42	2.99(+)	1.56	3.50(+)	1.66
2	7.57(+)	1.43	3.89(+)	1.62	3.19(+)	1.44
3	0.33	1.00	0.49	1.00	0.44(+)	<i>ca.</i> 1
4 <sup>b</sup>	22.3(-)	1.16	21.7(-)	1.12	28.5	1.00
5	4.09(+)	2.07	7.82(+)	2.76	4.14(+)	1.81
6	0.26	1.00	0.46(+)	<i>ca.</i> 1	0.49	1.00
7	0.30	1.00	0.34	1.00	0.41	1.00
8	0.77	1.00	0.66	1.00	1.18	1.00
9	0.77	1.00	0.87	1.00	1.70	1.00

<sup>a</sup> Column: 25 cm×0.20 cm ID. Flow rate: 0.1 mL/min. The signs in parentheses represent the circular dichroism detection at 254 nm of the first-eluted enantiomer. Eluent: *n*-hexane/2-propanol = 95/5, v/v. <sup>b</sup> Flow rate: 0.5 mL/min.

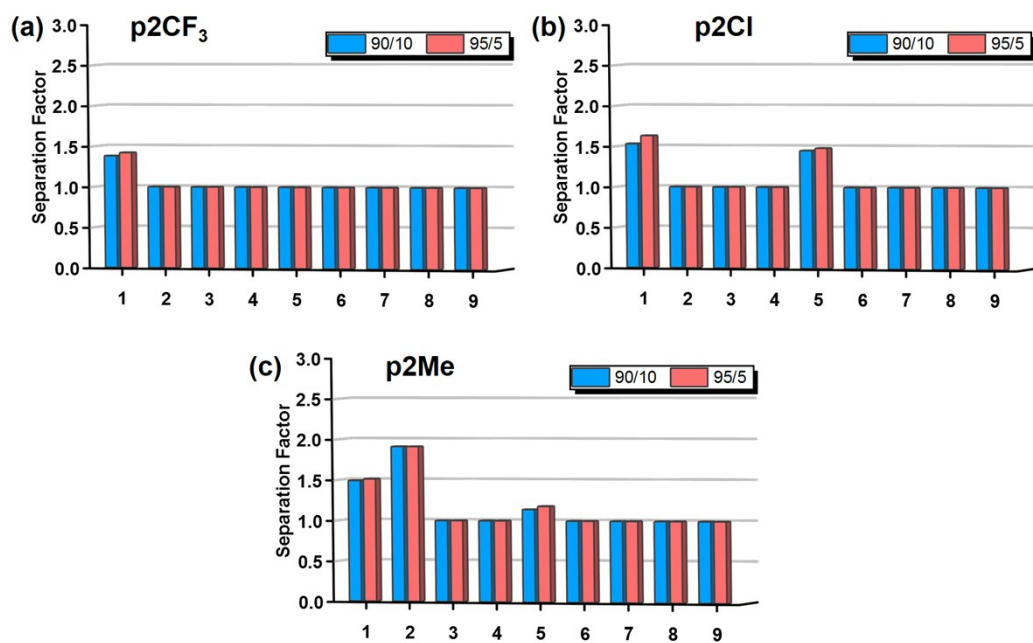


Figure S56. HPLC results of p2CF<sub>3</sub> (a), p2Cl (b) and p2Me (c).

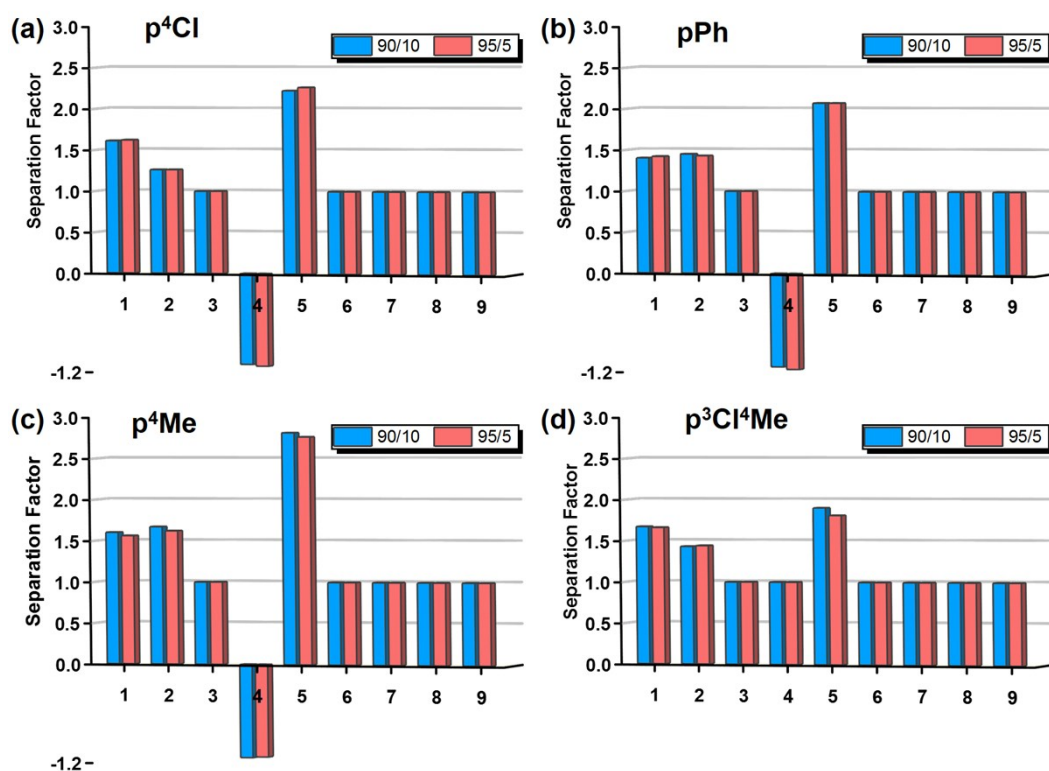


Figure S57. HPLC results of p<sup>4</sup>Cl (a), pPh (b), p<sup>4</sup>Me (c) and p<sup>3</sup>Cl<sup>4</sup>Me (d).

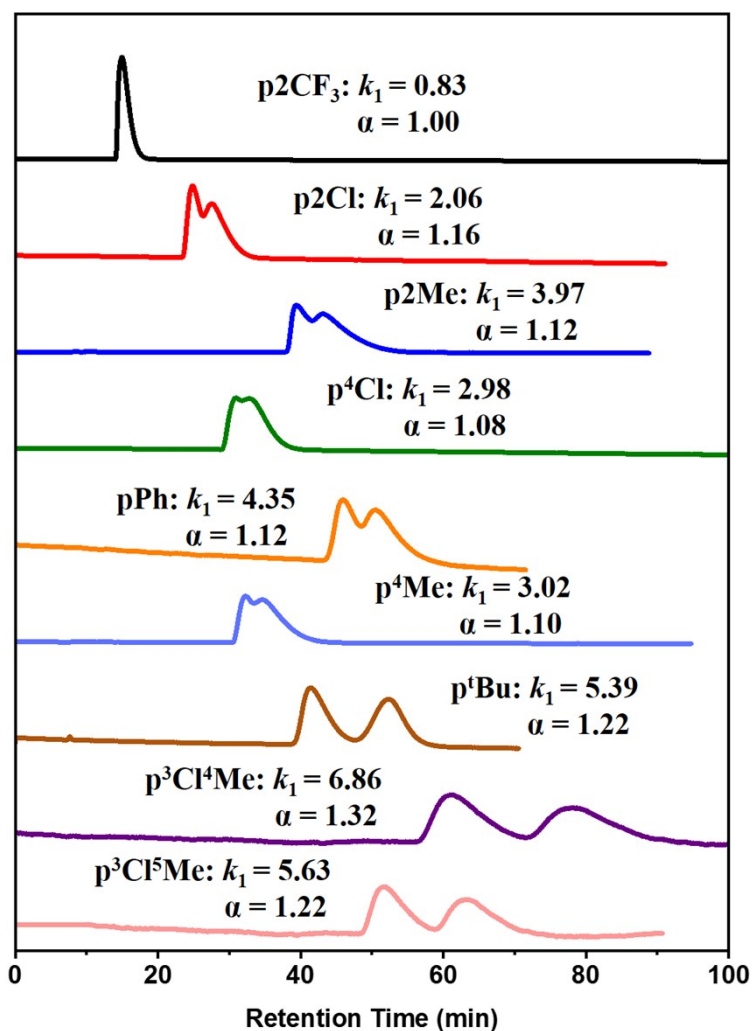
**Table S4.** HPLC results of **3** on nine CSPs under pure *n*-hexane.<sup>a</sup>

Racemates	p2CF <sub>3</sub>		p2Cl		p2Me		p <sup>4</sup> Cl		pPh	
	<i>k</i> <sub>1</sub>	$\alpha$								
<b>3</b>	0.83(+)	1.00	2.06(+)	1.16	3.97(+)	1.12	2.98(+)	1.08	4.35(+)	1.12

Racemates	p <sup>4</sup> Me		p <sup>t</sup> Bu		p <sup>3</sup> Cl <sup>4</sup> Me		p <sup>3</sup> Cl <sup>5</sup> Me	
	<i>k</i> <sub>1</sub>	$\alpha$	<i>k</i> <sub>1</sub>	$\alpha$	<i>k</i> <sub>1</sub>	$\alpha$	<i>k</i> <sub>1</sub>	$\alpha$
<b>3</b>	3.02(+)	1.10	5.39(+)	1.22	6.86(+)	1.32	5.63(+)	1.22

<sup>a</sup> Column: 25 cm×0.20 cm ID. Flow rate: 0.1 mL/min. The signs in parentheses represent the circular dichroism detection at 254 nm of the first-eluted enantiomer. Eluent: *n*-hexane.



**Figure S58.** HPLC chromatograms for resolution of racemate **3** on nine CSPs.

**Table S5.** HPLC results of nine enantiomers on two CSPs (95/5).<sup>a</sup>

Racemates	p <sup>4</sup> Cl		p <sup>4</sup> Cl-g	
	<i>k'</i> <sub>1</sub>	$\alpha$	<i>k'</i> <sub>1</sub>	$\alpha$
<b>1</b>	4.26(+)	1.62	2.18	1.00
<b>2</b>	3.57(+)	1.26	2.83	1.00
<b>3</b>	0.33	1.00	0.19	1.00
<b>4<sup>b</sup></b>	22.3(-)	1.12	11.0(-)	1.16
<b>5</b>	4.09(+)	2.26	5.81(+)	<i>ca.</i> 1
<b>6</b>	0.26	1.00	0.47	1.00
<b>7</b>	0.30	1.00	0.37	1.00
<b>8</b>	0.77	1.00	1.21	1.00
<b>9</b>	0.77	1.00	1.34	1.00

<sup>a</sup> Column: 25 cm × 0.20 cm ID. Flow rate: 0.1 mL/min. The signs in parentheses represent the circular dichroism detection at 254 nm of the first-eluted enantiomer. Eluent: *n*-hexane/2-propanol = 95/5, v/v. <sup>b</sup> Flow rate: 0.5 mL/min.

## 7. Computational Simulation

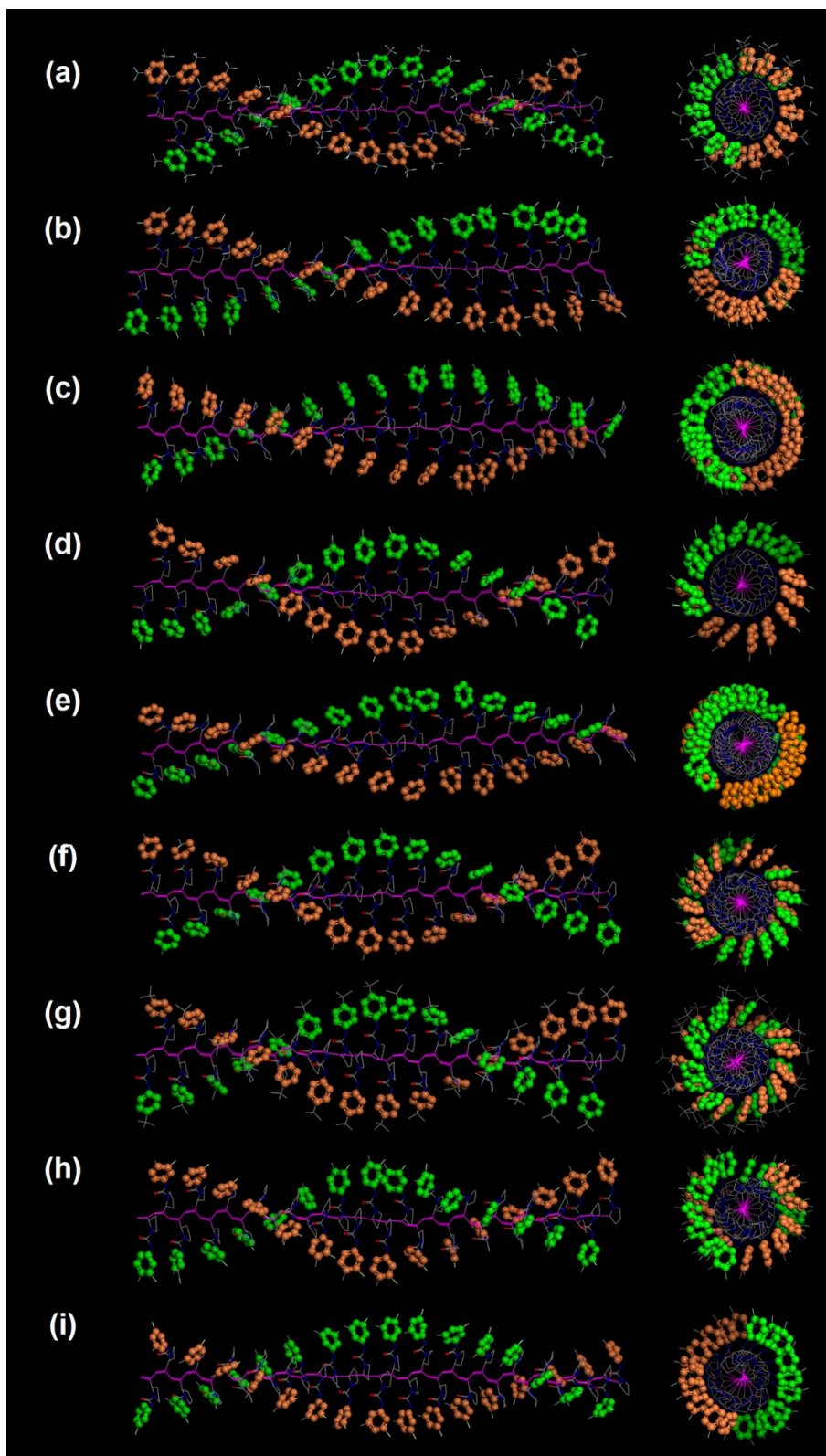


**Figure S59.** Possible 3D helical structures obtained from computational simulation: p2CF<sub>3</sub> (a), p2Cl (b), p2Me (c), p<sup>4</sup>Cl (d), pPh (e), p<sup>4</sup>Me (f), p<sup>1</sup>Bu (g), p<sup>3</sup>Cl<sup>4</sup>Me (h) and p<sup>3</sup>Cl<sup>5</sup>Me (i).

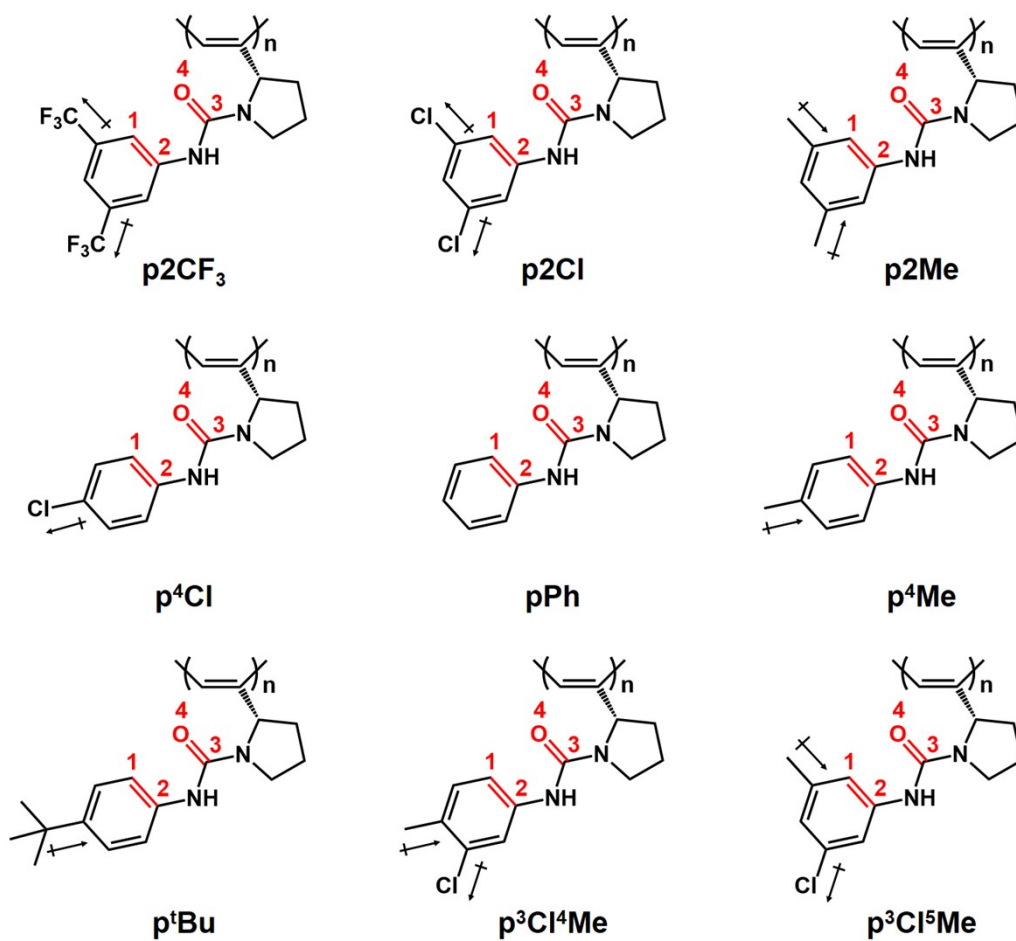


**Figure S60.** Torsional angle diagrams of nine polymers (selected atoms are marked in red).

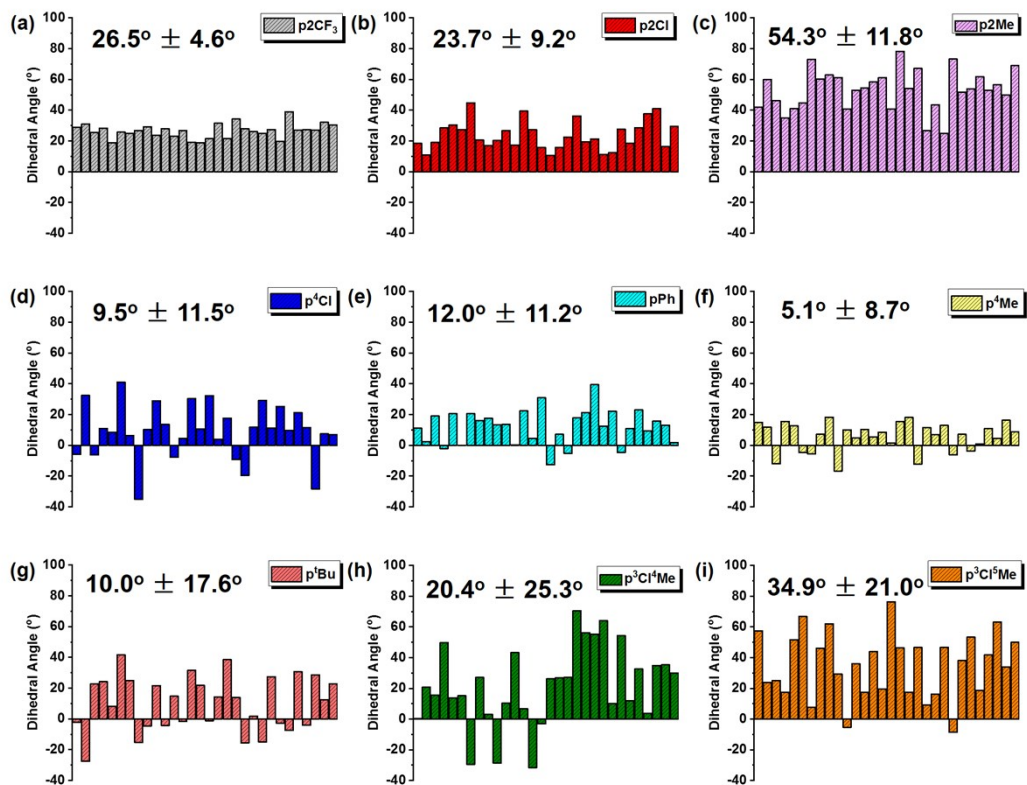


**Figure S61.** The simulation results of torsional angle for p2CF<sub>3</sub> (a), p2Cl (b), p2Me (c), p<sup>4</sup>Cl (d), pPh (e), p<sup>4</sup>Me (f), p<sup>4</sup>Bu (g), p<sup>3</sup>Cl<sup>4</sup>Me (h) and p<sup>3</sup>Cl<sup>5</sup>Me (i).

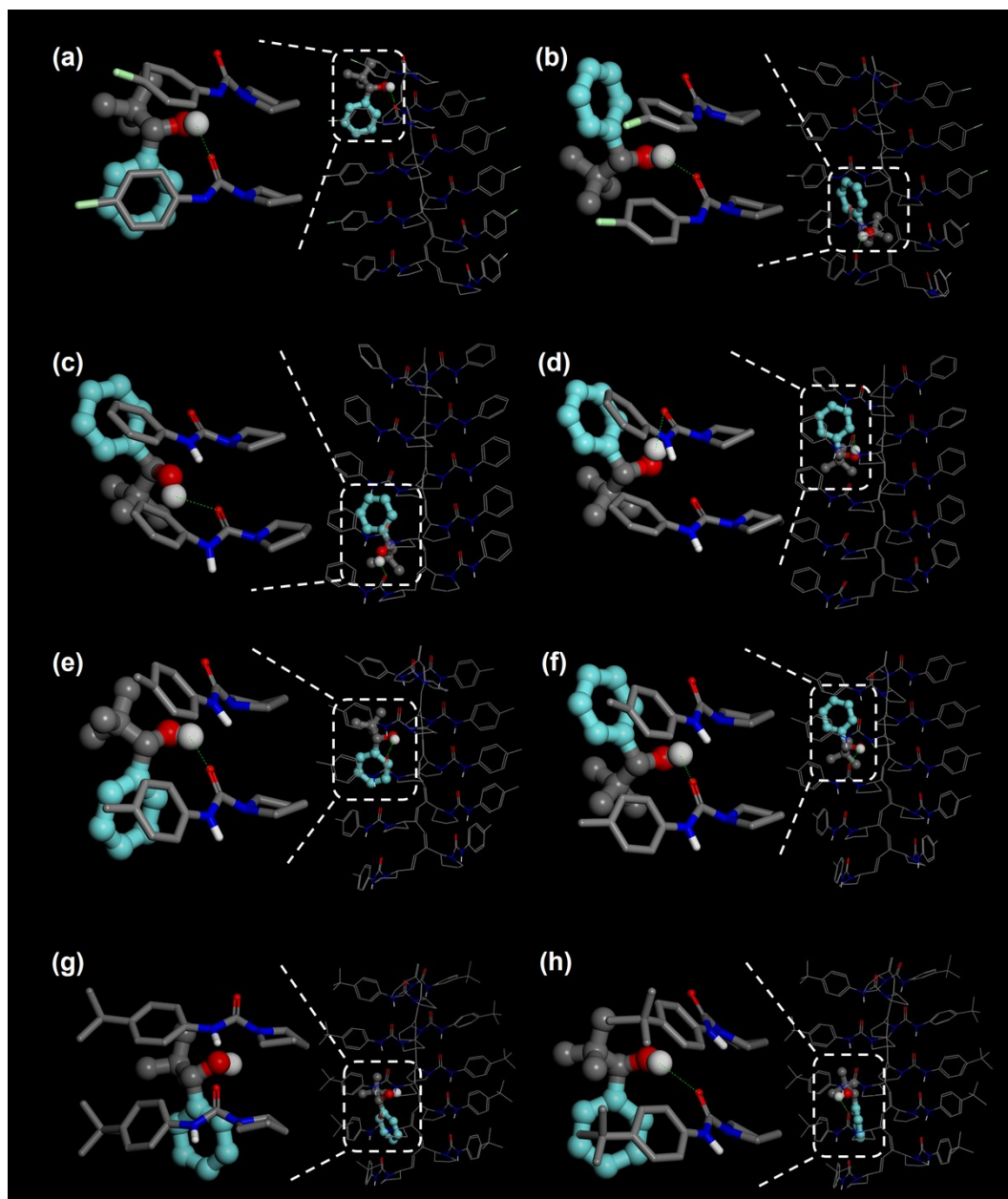


**Figure S62.** Molecular docking of the enantiomer (a) (+)-**3** and (b) (-)-**3** to p<sup>4</sup>Cl; (c) (+)-**3** and (d) (-)-**3** to pPh; (e) (+)-**3** and (f) (-)-**3** to p<sup>4</sup>Me; (g) (+)-**3** and (h) (-)-**3** to p<sup>4</sup>Bu. SA and CS were displayed in ball-stick model and line model, respectively. Atoms were colored as: C (gray), O (red), N (blue), H (white), Cl (green); aromatic groups of enantiomers (cyan); HBs were marked as green-colored dashed lines.

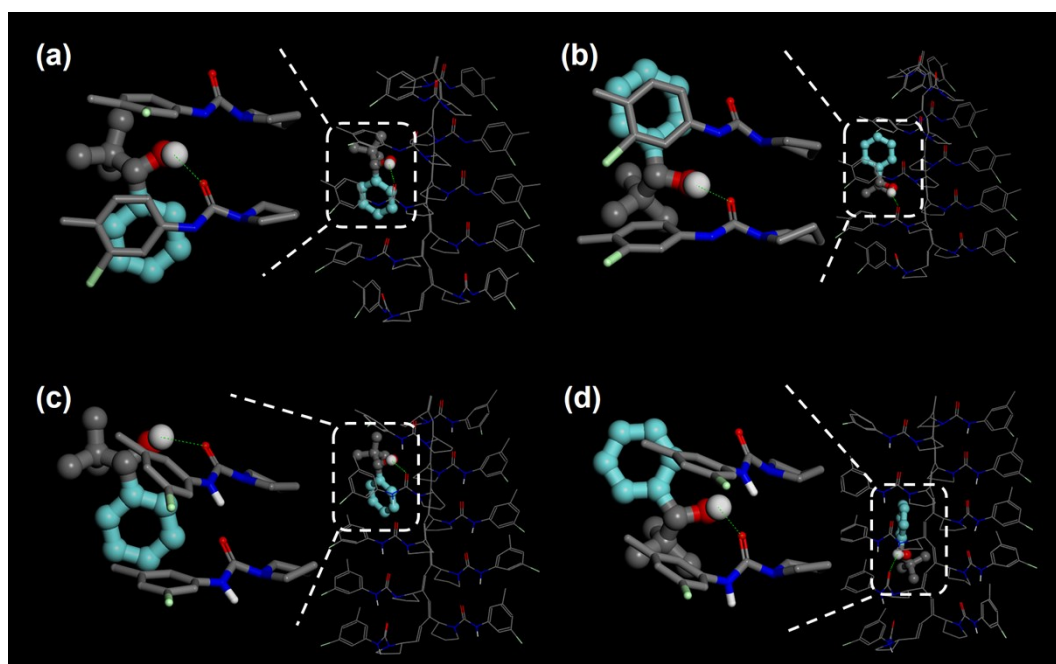


**Figure S63.** Molecular docking of the enantiomer (a) (+)-**3** and (b) (-)-**3** to  $p^3Cl^4Me$ ; (c) (+)-**3** and (d) (-)-**3** to  $p^3Cl^5Me$ . SA and CS were displayed in ball-stick model and line model, respectively. Atoms were colored as: C (gray), O (red), N (blue), H (white), Cl (green); aromatic groups of enantiomers (cyan); HBs were marked as green-colored dashed lines.

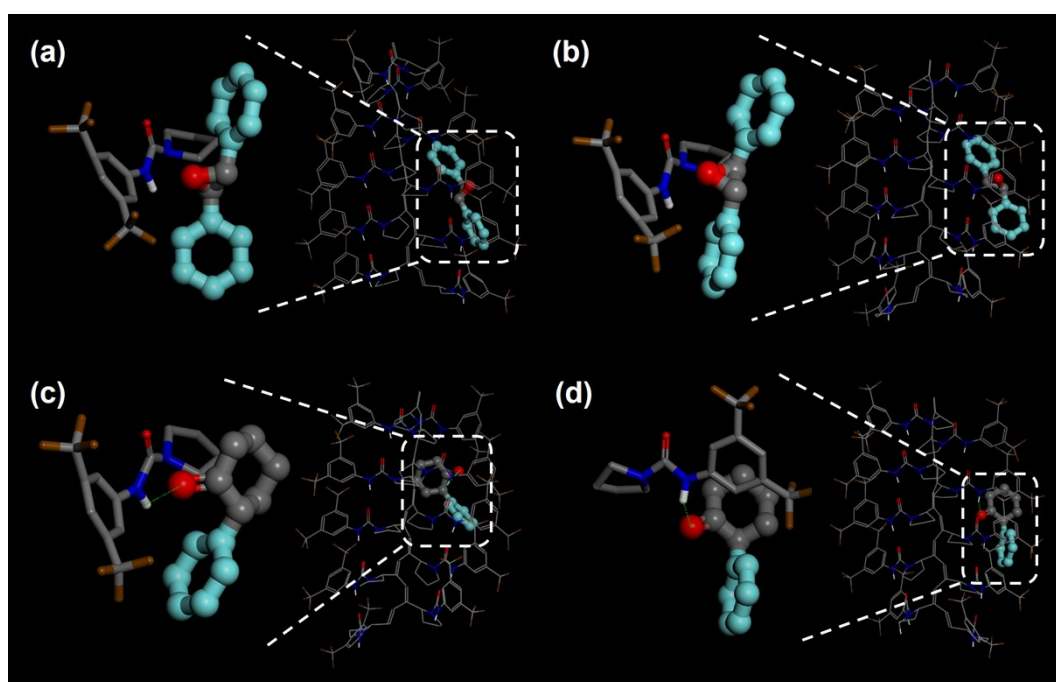


**Figure S64.** Molecular docking of the enantiomer (a) (+)-**7** and (b) (-)-**7** to  $p2CF_3$ ; (c) (+)-**8** and (d) (-)-**8** to  $p2CF_3$ . Atoms were colored as: C (gray), O (red), N (blue), H (white), F (brown); aromatic groups of enantiomers (cyan); HBs were marked as green-colored dashed lines.

**Table S6.** Molecular docking results of analyte **7-8**.

CSP	<b>(+)-7</b>		<b>(-)-8</b>		$\Delta\Delta E^c$ (kJ/mol)
	$d_{\text{HB}}$ (Å) <sup>a</sup>	$d_{\pi-\pi}$ (Å) <sup>b</sup>	$d_{\text{HB}}$ (Å)	$d_{\pi-\pi}$ (Å)	
<b>p2CF<sub>3</sub></b>	-	-	-	-	+0.07

CSP	<b>(+)-8</b>		<b>(-)-8</b>		$\Delta\Delta E^c$ (kJ/mol)
	$d_{\text{HB}}$ (Å)	$d_{\pi-\pi}$ (Å)	$d_{\text{HB}}$ (Å)	$d_{\pi-\pi}$ (Å)	
<b>p2CF<sub>3</sub></b>	2.648	-	2.676	-	+0.13

<sup>a</sup> The distance between hydrogen atom of SA hydroxyl and oxygen atom of CS urea. <sup>b</sup> The distance between centroid of SA and CS phenyl groups for face-to-face  $\pi-\pi$  interactions. <sup>c</sup> The difference in free energy of binding,  $\Delta\Delta E = \Delta E_{(+)} - \Delta E_{(-)}$ .

## 8. Reference

1. Shi, G.; Dai, X.; Zhou, Y.; Zhang, J.; Shen, J.; Wan, X. H. Synthesis and Enantioseparation of Proline-derived Helical Polyacetylenes as Chiral Stationary Phases for HPLC. *Polym. Chem.* **2020**, DOI: 10.1039/D0PY00205D.
2. Wang, S.; Feng, X. Y.; Zhao, Z. Z.; Zhang, J.; Wan, X. H. Reversible *Cis-Cisoid* to *Cis-Transoid* Helical Structure Transition in Poly(3,5-disubstituted phenylacetylene)s. *Macromolecules*, **2016**, *49*, 8407-8417.
3. Pisani, L.; Rullo, M.; Catto, M.; Candia, M.; Carrieri, A.; Cellamare, S.; Altomare, C.D. Structure–property Relationship Study of the HPLC Enantioselective Retention of Neuroprotective 7-[(1-alkylpiperidin-3-yl)methoxy]coumarin Derivatives on an Amylose-based Chiral Stationary Phase. *J. Sep. Sci.*, **2018**, *41*, 1376-1384.
4. Shen, J.; Wang, F.; Bi, W. Y.; Liu, B.; Liu, S. Y.; Okamoto, Y. Synthesis of Cellulose Carbamates bearing Regioselective Substituents at 2,3- and 6-positions for Efficient Chromatographic Enantioseparation. *J. Chromatogr. A.*, **2018**, *1572*, 54-61.